Geochemical diversity in first rocks examined by the Curiosity Rover in Gale Crater: Evidence for and significance of an alkali and volatile-rich igneous source

M. E. Schmidt, J. L. Campbell, R. Gellert, G. M. Perrett, A. H. Treiman, D. L. Blaney, A. Olilla, F. J. Calef Iii, L. Edgar, B. E. Elliott, et al.

Geochemical diversity in first rocks examined by the Curiosity Rover in Gale Crater: Evidence for and significance of an alkali and volatile-rich igneous source

M. E. Schmidt,[1] J. L. Campbell,[2] R. Gellert,[2] G. M. Perrett,[2] A. H. Treiman,[3] D. L. Blaney,[4] A. Olilla,[5] F. J. Calef III,[4] L. Edgar,[6] B. E. Elliott,[7] J. Grotzinger,[4,8] J. Hurowitz,[9] P. L. King,[10] M. E. Minitti,[11] V. Sautter,[12] K. Stack,[8] J. A. Berger,[13] J. C. Bridges,[14] B. L. Ehlmann,[4,8] O. Forni,[15] L. A. Leshin,[16] K. W. Lewis,[17] S. M. McLennan,[17] D. W. Ming,[18] H. Newsom,[5] I. Pradler,[2] S. W. Squyres,[19] E. M. Stolper,[8] L. Thompson,[7] S. VanBommel,[2] and R. C. Wiens[20]

Received 9 July 2013; revised 27 November 2013; accepted 3 December 2013; published 16 January 2014.

[1] The first four rocks examined by the Mars Science Laboratory Alpha Particle X-ray Spectrometer indicate that Curiosity landed in a lithologically diverse region of Mars. These rocks, collectively dubbed the Bradbury assemblage, were studied along an eastward traverse (sols 46–102). Compositions range from Na- and Al-rich mugearite Jake_Matijevic to Fe-, Mg-, and Zn-rich alkali-rich basalt/hawaiite Bathurst_Inlet and span nearly the entire range in FeO* and MnO of the data sets from previous Martian missions and Martian meteorites. The Bradbury assemblage is also enriched in K and moderately volatile metals (Zn and Ge). These elements do not correlate with Cl or S, suggesting that they are associated with the rocks themselves and not with salt-rich coatings. Three out of the four Bradbury rocks plot along a line in elemental variation diagrams, suggesting mixing between Al-rich and Fe-rich components. ChemCam analyses give insight to their degree of chemical heterogeneity and grain size. Variations in trace elements detected by ChemCam suggest chemical weathering (Li) and concentration in mineral phases (e.g., Rb and Sr in feldspars). We interpret the Bradbury assemblage to be broadly volcanic and/or volcaniclastic, derived either from near the Gale crater rim and transported by the Peace Vallis fan network, or from a local volcanic source within Gale Crater. High Fe and Fe/Mn in Et_Then likely reflect secondary precipitation of Fe^{3+} oxides as a cement or rind. The K-rich signature of the Bradbury assemblage, if igneous in origin, may have formed by small degrees of partial melting of metasomatized mantle.

Citation: Schmidt, M. E., et al. (2014), Geochemical diversity in first rocks examined by the Curiosity Rover in Gale Crater: Evidence for and significance of an alkali and volatile-rich igneous source, *J. Geophys. Res. Planets*, *119*, 64–81, doi:10.1002/2013JE004481.

[1]Department of Earth Sciences, Brock University, St. Catharines, Ontario, Canada.
[2]Department of Physics, University of Guelph, Guelph, Ontario, Canada.
[3]Lunar Planetary Science Institute, Houston, Texas, USA.
[4]Jet Propulsion Laboratory, Pasadena, California, USA.
[5]Institute of Meteoritics, University of New Mexico, Albuquerque, New Mexico, USA.
[6]Arizona State University, Tempe, Arizona, USA.
[7]Department of Earth Sciences, University of New Brunswick, Fredericton, New Brunswick, Canada.
[8]California Institute of Technology, Pasadena, California, USA.
[9]Department of Geosciences, SUNY Stony Brook, Stony Brook, New York, USA.
[10]Research School of Earth Sciences, Australia National University, Canberra, ACT, Australia.
[11]Applied Physics Laboratory, Johns Hopkins University, Laurel, Maryland, USA.
[12]Museum National D'Histoire Naturelle, Paris, France.
[13]Department of Earth Sciences, University of Western Ontario, London, Ontario, Canada.
[14]Space Research Centre, Department of Physics and Astronomy, University of Leicester, Leicester, Leicestershire, UK.
[15]Institut de Recherch en Astrophysique et Planetologie, Université Paul Sabatier, UPS-OMP, Toulouse, France.
[16]School of Science, Rensselear Polytechnic Institute, Troy, New York, USA.
[17]Princeton University, Princeton, New Jersey, USA.
[18]NASA Johnson Space Center, Houston, Texas, USA.
[19]Department of Astronomy, Cornell University, Ithaca, New York, USA.
[20]Los Alamos National Laboratory, Los Alamos, New Mexico, USA.

Corresponding author: M. E. Schmidt, Department of Earth Sciences, Brock University, St. Catharines, Ontario, L2S 3A1, Canada. (mschmidt2@brocku.ca)

2169-9097/15/10.1002/2013JE004481

1. Introduction

[2] Each landing site on Mars is unique and contributes to our understanding of the diversity of Martian rocks and soils and the wide range of geologic processes and conditions that generated them [e.g., *Squyres et al*., 2004a; *Squyres et al*., 2004b; *Smith et al*., 2009]. Gale Crater, the site selected for the Mars Science Laboratory (MSL) Curiosity rover, is no exception [*Grotzinger et al*., 2012]. An important component of the MSL payload is the Alpha Particle X-ray spectrometer (APXS) on the rover's arm, which measures elemental compositions of ~1.7 cm diameter spots on rock surfaces and soils [*Gellert et al*., 2013]. The MSL APXS is the fourth such instrument to have landed on Mars and allows direct comparison with rocks and soils from previous Mars landing sites [e.g., *Rieder et al*., 2004; *Gellert et al*., 2006; *Brückner et al*., 2003].

[3] The first sign of Gale's unique geochemistry came from the ChemCam instrument, which uses laser-induced breakdown spectroscopy (LIBS) to measure chemical compositions of 200–400 μm spots [*Maurice et al*., 2012]. ChemCam analyses are complementary to those done by the APXS and give an indication of the degree of geochemical heterogeneity, grain size, and mineral components. The compositions of soils and rocks examined by the ChemCam early along the rover's traverse are variable and include spots with high Si, Al, and K, consistent with feldspar-rich components [*Meslin et al*., 2013].

[4] During Curiosity's eastward traverse from the landing site that is Bradbury Landing (All of the small-scale features' names in this paper are informal and are not approved by the International Astronomical Union) toward Glenelg, a contact between three distinct geomorphic units (sols 46–102; Figure 1), the APXS examined four rocks and one soil. We, hereafter, refer to the four analyzed rocks as the "Bradbury assemblage," a classification without implied genetic connection, and present their chemical compositions, make inferences about their petrologic origin, and place them in a broader geologic context within Gale Crater. We present evidence that the Bradbury assemblage is composed of volcanic, volcaniclastic, and/or relatively immature sedimentary rocks. Compared to other Martian rocks, the Bradbury assemblage is chemically diverse and expands the range of known Martian rock compositions to include high alkalis (up to 2.9 wt% K_2O), high Fe (up to 26.3 wt% FeO*; all Fe reported as FeO*), and high Mn (up to 0.8 wt% MnO). The discovery of such high-K rocks in Gale Crater has important implications for the composition of the Martian crust and for thermal and petrological modeling of the evolution of the Martian mantle.

2. Geologic Traverse

[5] Gale Crater, a 155 km diameter crater of Late Noachian/Early Hesperian age, is located in the Aeolis region on the hemispheric dichotomy boundary between the heavily cratered southern highlands and smooth northern lowlands. The crater rim varies in elevation from ~3000 m on the northern crater rim to ~500 m on the southern crater rim. A 5 km thick sequence of strata, known informally as Mt. Sharp, occurs at the center of the crater. Phyllosilicate, sulfate, and hematite-bearing strata compose the lower portion of Mt. Sharp and are unconformably overlain by the upper formation with regular bedding and no hydrated mineral signatures [*Milliken et al*., 2010]. The mineralogical and morphological diversity present at Mt. Sharp suggests a range of depositional processes and environments that may span several billion years [*Grotzinger and Milliken*, 2012] and is the primary target of the MSL mission.

[6] The floor of Gale Crater contains a range of rock units identified from HiRISE High Resolution Imaging Science Experiment (surface morphology) and CRISM (Compact Reconnaissance Imaging Spectrometer for Mars; visible-near infrared spectra) data [*Anderson and Bell*, 2010; *Calef et al*., 2013; *Rice et al*., 2013; *Sumner et al*., 2013] that are inferred to be largely sedimentary and variably affected by impact processes. These sedimentary units may be sourced from volcanic and/or igneous rock exposed at or near the Gale Crater rim, which is 5 km tall relative to the crater floor, although a more local volcanic source from within Gale Crater is possible, as are distal, large centers of volcanism, such as Elysium Mons, which is located ~1500 km directly north of Gale. Also, within 20 km of Gale Crater, there are outcrops of possible pyroclastic ashfall tuff or ash flows from the Medusae Fossae Formation [*Kerber et al*., 2011; *Zimbelman and Scheidt*, 2012]. These rocks have been proposed to make up units within Mt. Sharp [*Scott and Chapman*, 1995; *Thomson et al*., 2011; *Zimbelman and Scheidt*, 2012] and may also contribute material to the region near the Curiosity landing site.

[7] In August of 2012, the Curiosity rover touched down in Gale Crater at Bradbury Landing, several kilometers north of Mt. Sharp and ~14 km south of the apex of the Peace Vallis fan, a large, low gradient fan in Gale Crater [*Palucis et al*., 2013; *Sumner et al*., 2013; *Williams et al*., 2013]. This alluvial fan is fed by Peace Vallis, a ~32 km long, ~40 m wide channel that incises the northwestern rim of Gale Crater and empties onto a fan defined primarily by convex contours within an enclosed basin that includes Bradbury Landing and Glenelg. The gully system feeding the fan is estimated to have removed ~500(10^6) m^3 of material, and the current fan covers an area of ~ 80 km^2 [*Palucis et al*., 2013; *Sumner et al*., 2013].

[8] After arriving at Bradbury Landing, the Curiosity rover drove east (Figure 1) toward an area informally named Glenelg, which represents the juxtaposition of three geomorphic units: a dark-toned hummocky plains unit (HP), a dark-cratered unit, and a light-toned, bedded, fractured unit (BF) [*Grotzinger et al*., 2013]. The eastward traverse took Curiosity downhill across a geomorphic unit (HP) characterized in HiRISE images by its darker tone, hummocky topography, smoother appearance, and relatively few retained craters compared to surrounding units. Its stratigraphic relationship to the other two units is unclear at this time [*Grotzinger et al*., 2013].

[9] The first bedrock encountered by Curiosity was pebble conglomerate of likely fluvial origin exposed from beneath the regolith by the descent-stage thrusters during landing [*Williams et al*., 2013]. Similar conglomerates found along the early part of the traverse were examined by ChemCam [*Ollila et al*., 2013a; *Sautter et al*., 2014] but not by instruments on the rover's arm. Use of the arm was first possible on sol 46 when the rover encountered the rock Jake_Matijevic, a large (~50 cm), coherent, visually homogeneous piece of float that appears to be unrelated to nearby bedrock outcrops. Continuing east, the sol 53 drive ended with Curiosity parked over an exposure of fine-grained bedrock, and on the next sol, it was able to extend the arm to examine

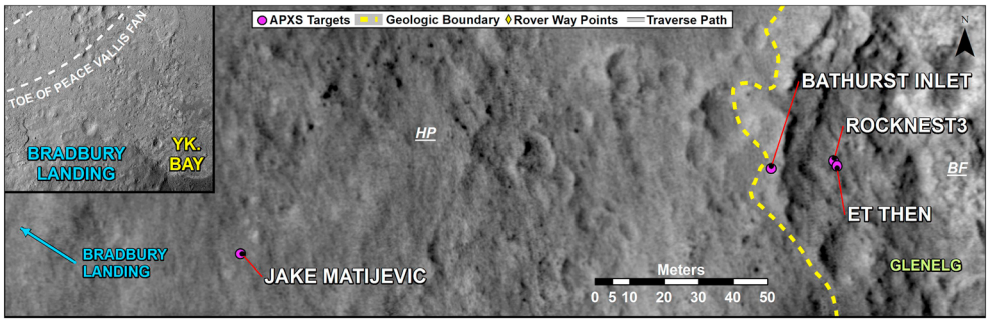

Figure 1. Rover traverse on HiRISE base map with the locations of the APXS rock targets indicated. Yellow dashed line defines the geologic boundary between clast-rich substrate of the hummocky plains unit (HP) and the near flat-lying layered bedrock of the light-toned fractured unit (BF) to the east. Inset map shows the rover's traverse (~400 m as a Martian crow would fly) from Bradbury Landing to the Rocknest sand shadow and Yellowknife (YK.) Bay in relation to the southern topographic expression of the Peace Vallis Fan.

rock target Bathurst_Inlet with the APXS and Mars Hand Lens Imager (MAHLI). Bathurst_Inlet represents the uppermost exposed layer of a package of near flat-lying bedded rocks (BF) that are exposed to the east (Figure 1 [*Grotzinger et al*., 2013]). Orbital mapping and textural characteristics observed from Mastcam imaging of the Bathurst_Inlet outcrop link it to the Shaler outcrop (examined sol ~320), and it has been mapped as the Glenelg member of the BF [*Grotzinger et al*., 2013].

[10] The rover next drove to the Rocknest sand shadow, where it spent nearly 50 sols parked on the leeward side of a small topographic high. Here, the rover used its sample acquisition and sample handling system (SA/SPaH) to collect samples from an aeolian deposit and deliver them to the CheMin and SAM (Sample Analysis at Mars) instruments [*Blake et al*., 2013; *Leshin et al*., 2013]. At this location, the APXS examined four soil targets, including one reported here called Portage. This soil is similar in composition to soils examined at other Martian sites, and it is inferred to be representative of the modern aeolian component in Gale Crater with as much as a 15% local bedrock component [*Yen et al*., 2013]. While at Rocknest, ChemCam conducted a detailed survey of nearby rock targets [*Tokar et al*., 2013]. The APXS also examined two rocks: Et_Then, a float rock located near the rover's front left wheel, and Rocknest_3, which appears to be a dislodged piece of the local bedrock, on sols 91 and 102, respectively. Vuggy rock textures, compositional characteristics, and orbital mapping relate, with some uncertainty, the Rocknest rocks to the Point Lake outcrop (examined sol ~304), within the middle of the Glenelg member [*Grotzinger et al*., 2013; *McLennan et al*., 2013].

3. Methods

[11] Curiosity carries a payload that enables geologic and geochemical investigations of rocks and soils it encounters along its traverse. Traverse elements include roving capability, navigation and science cameras, and the geochemical analytical instruments APXS and ChemCam [*Grotzinger et al*., 2012]. Although our focus here is on the APXS results of rock targets, microtextural and dust coverage information from the MAHLI [*Edgett et al*., 2012] and complementary geochemical information provided by the ChemCam enter into our interpretations.

3.1. APXS

[12] The MSL APXS uses radioactive ^{244}Cm sources that excite geologic samples via PIXE (particle-induced X-ray emission) and X-ray fluorescence. Characteristic X-rays are emitted from the sample as a result of these two processes and are detected by the APXS instrument. The characteristic X-ray energies are unique for each element present in the target, and their intensities are used to determine the abundances of major, minor, and some trace (Cr, Ni, Zn, Br, and Ge) elements [*Campbell et al*., 2012; *Gellert et al*., 2013]. Penetration depths to the region above which 90% of the observed X-rays originate increase as a function of Z and range from 2 to 80 µm for Na to Fe. A calibration standard [*Campbell et al*., 2013; *Thompson et al*., 2013] was sent to Mars with the rover to verify that the APXS calibration produced on Earth remains valid on Mars. A Peltier cooler permits the recording of daytime spectra with integrations as short as 10 min. An aluminum contact sensor allows for reproducible instrument placement heights, which is valuable for determining accurate elemental abundances. The diameter of an APXS field of view (FOV) in contact is 1.7 cm, but it increases (~45° cone) with increasing standoff.

[13] Integration parameters for the eight APXS observations of the five targets included in this study are presented in Table 1. Jake_Matijevic was examined in two spots (JM1 and JM2); JM2 was examined twice at different times of day. Two spots were also examined on Bathurst Inlet ("BI_For_Real" and "BI_Top"). Single spots were examined on Et_Then and Rocknest_3. APXS analyses of all rocks, except for Et_Then, were conducted in contact, meaning the contact sensor was touching the rock surfaces. Et_Then was examined at a less favorable distance of approximately 5.4 cm standoff due to the awkward orientation of the rock in relation to the rover's position. The Portage soil was examined at 2 cm standoff to prevent possible contamination of the APXS sources and detector with the fine-grained material.

[14] We reduced the APXS data using two independent data analysis methods. The first (the "Gellert method") builds on the peak-fitting and calibration routine that was developed for the Mars Exploration Rover (MER) APXS analyses (Tables 2 and 3 [*Gellert et al*., 2006]); the second (the "GUAPX" method) is based upon the fundamental physics

Table 1. APXS Integration Parameters[a]

	Sol	Standoff (cm)	Duration (min)	Temperature (°C)	Pressure (Pa)[b]	FWHM (Mn) (eV)[c]
Jake_Matijevic						
JM1	46	0	30	−3.5	760	201
JM2 (daytime)	47	0	12	−2	759	209
JM2 (nighttime)	47	0	30	−55	758	144
Bathurst_Inlet						
Bathurst_Inlet_For_Real	54	0	20	−5.1	767	193
Bathurst_Inlet_Top	54	0	20	−3.5	767	210
Et_Then	91	5.4	120	−61.2	818	137
Rocknest_3	102	0	22	−0.3	833	224
Portage (soil)	89	2.0	155	−64.3	814	138

[a]All analyses are of unbrushed rock surfaces, unless noted as a soil.
[b]Atmospheric pressure was determined by the REMS [*Harri et al*., 2013].
[c]FWHW (Mn) is the full-width-at-half-maximum energy resolution centered on the Mn peak [*Gellert et al*., 2006].

of X-ray and alpha particle interactions with matter and resembles the approaches generally employed for X-ray fluorescence and electron microprobe analysis (Tables 4 and 5 [*Campbell et al*., 2012]). We limit the GUAPX results to the four best analyses, where the energy resolution is <180 eV (full width at half maximum or FWHM; Table 1).

[15] The major differences between these data-reduction methods are their different approaches to calibration, spectrum fitting, and matrix corrections. Light-element results are sensitive to the atmospheric pressure, which is assumed to be 8 mbar in the Gellert method; in the GUAPX method, measured pressure as measured by REMS (Rover Environmental Monitoring Station) was used [*Harri et al*., 2013]. In each method, varying standoff distances are taken into account by a geometric normalization such that the total oxide content is normalized to 100 wt%. Laboratory calibration efforts on powdered geological reference materials are ongoing, and the current best estimates of overall analytical accuracies are ~±3% (relative) for Si; ±5–10% for Al, Ca, Mn, and Fe; ±10–15% for Na, P, S, and K; ±15–20% for Mg, Ti, Cr, Ni, Zn, Ge, and Br; and ~±30% for Cl. For the following discussions, we report statistical (2σ) errors generated by the respective spectrum-fitting routines (Tables 3 and 5) because they represent gradual changes in mineral abundances, where the precision of the APXS method allows insight into the elemental composition of the involved minerals. These errors are functions of the overall spectral intensity and thus reflect duration and standoff, and they are also increased by increasing temperature which causes greater peak overlap. Additional uncertainties associated with higher standoff include the effect of atmospheric pressure on light-element X-ray absorption, the increased FOV, and interference from background components (P, Ti, K [*Campbell*, 2012]). Statistical errors are significantly smaller than the uncertainties associated with the calibration; the lighter elements especially show larger spreads for geological reference materials relative to their certificate values that reflect the influence of the rock mineralogy on the matrix effects [*Gellert et al*., 2006; *Campbell et al*., 2012; Gellert et al., manuscript in preparation].

3.2. ChemCam

[16] The ChemCam instrument provides a complementary data set that can be used to understand chemical heterogeneity and potential mineralogy. ChemCam utilizes laser-induced breakdown spectroscopy (LIBS) to provide elemental composition at distances up to 7 m from the rover [*Maurice et al*., 2012; *Wiens et al*., 2012]. Analysis spot size ranges from 350 μm to 550 μm, increasing with distance from the mast. The laser repeatedly fires upon a given analysis spot (generally from 30 to 50 laser shots), and the emission spectra from each laser shot are recorded. Analysis of ChemCam data can be done by averaging spot compositions or by looking at the data on a shot by shot basis. The first five shots are typically not included in rock analysis due to the potential contamination by dust and other fine-grained material. In general, compositions tend to stabilize after the first five laser firings [*Blaney*

Table 2. Compositions of First Four Rocks and One Soil in Gale Crater Determined by APXS by Gellert Method[a]

	SiO_2	TiO2	Al_2O_3	FeO*[b]	MnO	MgO	CaO	Na_2O	K_2O	P_2O_5	Cr_2O_3	Cl	SO_3	Ni	Zn	Br	Ge
	(wt%)													(ppm)			
Jake_Matijevic																	
JM1	50.68	0.50	16.14	9.44	0.14	3.63	6.09	7.09	2.22	0.50	0.03	0.88	2.46	22	216	88	9
JM2 (daytime)	49.30	0.65	14.59	10.61	0.17	4.56	6.54	6.61	2.01	0.60	0.09	1.03	3.05	0	341	94	4
JM2 (nighttime)	48.88	0.73	14.64	10.94	0.21	4.60	6.78	6.59	1.89	0.85	0.04	0.95	2.81	59	318	107	8
Bathurst_Inlet																	
BI_For_Real	43.69	1.11	7.90	21.91	0.78	8.60	6.30	2.24	2.18	0.83	0.41	0.74	3.08	395	1332	14	81
BI_Top	43.89	1.04	8.03	20.82	0.43	8.78	6.43	2.14	2.88	0.89	0.35	0.81	3.30	321	1210	39	46
Et_Then	45.06	0.73	8.41	26.33	0.39	4.19	4.27	2.95	1.57	0.99	0.08	0.79	4.06	227	486	50	18
Rocknest_3	45.98	0.96	10.51	18.38	0.45	5.33	6.06	4.02	1.86	1.08	0.25	0.88	4.05	364	888	62	102
Best mix[c]	*46.05*	*0.94*	*10.89*	*17.11*	*0.53*	*6.86*	*6.52*	*4.16*	*2.05*	*0.84*	*0.25*	*0.83*	*2.96*	*247*	*886*	*55*	*49*
Portage (soil)	42.88	1.19	9.43	19.19	0.41	8.69	7.28	2.72	0.49	0.94	0.49	0.69	5.45	446	337	26	15

[a]Gellert method is based on calibration of *Gellert et al*. [2006] of the MER APXS and applied to MSL. All analyses are of unbrushed rock surfaces, unless noted as a soil. See Figure 1 for location information.
[b]Total Fe is reported as FeO*.
[c]The best mix was calculated as 44% JM2 (nighttime) and 56% BI_For_Real and is ±12%, excepting MgO, P_2O_5, Ni, and Ge.

Table 3. Standard Error (2σ) for Compositions of First Four Rocks Determined by APXS by the Gellert Method[a]

	SiO_2	TiO2	Al_2O_3	FeO*	MnO	MgO	CaO	Na_2O	K_2O	P_2O_5	Cr_2O_3	Cl	SO_3	Ni	Zn	Br	Ge
	(wt %)													(ppm)			
Jake_Matijevic																	
JM1	0.61	0.03	0.46	0.07	0.01	0.35	0.07	0.30	0.04	0.07	0.01	0.03	0.09	17	13	8	8
JM2 (daytime)	0.88	0.06	0.69	0.11	0.02	0.58	0.11	0.50	0.06	0.12	0.03	0.05	0.16	0	25	11	10
JM2 (nighttime)	0.55	0.03	0.21	0.09	0.01	0.12	0.08	0.14	0.03	0.04	0.01	0.03	0.08	17	15	7	6
Bathurst_Inlet																	
BI_For_Real	0.58	0.04	0.37	0.15	0.03	0.33	0.08	0.27	0.04	0.07	0.03	0.03	0.11	38	38	8	15
BI_Top	0.57	0.04	0.38	0.13	0.02	0.35	0.08	0.31	0.05	0.08	0.03	0.03	0.11	32	32	10	14
Et_Then	0.50	0.05	0.19	0.17	0.03	0.16	0.10	0.18	0.05	0.08	0.03	0.06	0.17	84	53	16	29
Rocknest_3	0.77	0.04	0.58	0.13	0.03	0.52	0.09	0.45	0.05	0.15	0.03	0.04	0.16	37	30	10	17
Portage (soil)	0.47	0.03	0.14	0.12	0.01	0.14	0.07	0.10	0.01	0.03	0.02	0.02	0.10	29	17	6	8

[a]Gellert method is based on calibration of *Gellert et al*. [2006] of the MER APXS and applied to MSL. Standard error is 2 sigma statistical.

et al., 2013; *Lanza et al*., 2013]. Transitions between grains of different materials have been observed as a function of depth, and so the spectra are inspected on a shot by shot basis before averaging [*Meslin et al*., 2013]. Multiple locations are required to obtain an understanding of the bulk composition and chemical heterogeneity, and these spots are typically acquired as small rasters in azimuth and elevation (e.g., 1×5, 3×3) with steps between points of a few millirads. For cross comparison to APXS targets, a large number of observations are generally desired due to the differences in areal coverage. The ChemCam instrument thus allows assessment of rock variability as a function of depth into the rock, between locations on a rock surface, and between different rocks.

[17] Elemental abundances can be calculated from ChemCam spectra using a partial least squares (PLS) approach [*Clegg et al*., 2009] that involves comparison to a spectral library of ~70 certified standards collected on the flight instrument prior to launch. Uncertainties were determined by performing a leave-one-out cross validation of the training sets [e.g., *Wiens et al*., 2013; *Lasue et al*., 2013]. Because the PLS method relies on training sets, elements that are in much higher or lower abundance than in members of the training set may be systematically overestimated or underestimated. This is notably true of the alkalis (Na and K), which are underestimated by the PLS for the Bradbury assemblage relative to APXS abundances due to a dearth of high alkali standards in the prelaunch spectral training set. As an alternate approach, independent component analysis (ICA) is a multivariate technique used to classify components of the spectra [*Forni et al*., 2013]. Components corresponding to the major peaks of different elements can be observed separately to determine their trends.

[18] Minor and trace elements detected by the ChemCam instrument in the Bradbury assemblage include Li, Sr, Rb Ba, Mn, and Cr. Li, Sr, and Ba abundances were determined from a univariate peak area linear regression method, while Rb abundances are from a PLS method modified from the major element calibration discussed in *Wiens et al*. [2013]. The modification consists of a reduction in the input matrix that includes only those wavelengths that correspond to the modeled element. Details on the detection and calibration of the trace elements are given by *Ollila et al*. [2013b]. Models for the transition metals Mn and Cr are in progress, and preliminary observations are presented here. The root mean square (RMS) error of prediction and concentration ranges for minor and trace elements in the APXS rock targets are presented in Table 6.

4. Results

4.1. Rock Descriptions

[19] The Bradbury assemblage includes the first four rocks examined by the APXS. The typical Martian red-brown dust variably covers all rock surfaces. The APXS examined only unbrushed rock surfaces during the first 102 sols, and so compositions reported for that period include some degree of dust contamination. The ChemCam data after the first one to five shots represent the underlying rock material.

4.1.1. Jake_Matijevic

[20] Jake_Matijevic is a dark gray, fine- to medium-grained rock that is roughly pyramidal in shape (~50 cm tall and its three base edges are ~50 cm long; Figures 2a and 2b). Upper surfaces display rounded hollows that likely formed by wind erosion, and pits (<1–3 mm) that are possible vesicles. The lowest 5 cm of the rock has smoother, slightly indented surfaces that may either reflect primary layering, chemical weathering, or the effects of wind erosion. Projecting upward from the rock's base are vertical fractures (~10 cm long). Inspection of MAHLI images with varying illumination provided by MAHLI's white light light-emitting diodes suggests the presence of reflective minerals or grains,

Table 4. APXS Analyses of First Four Rocks and One Soil in Gale Crater by GUAPX[a]

	SiO_2	TiO2	Al_2O_3	FeO*[b]	MnO	MgO	CaO	Na_2O	K_2O	P_2O_5	Cr_2O_3	Cl	SO_3	Ni	Zn	Br	Ge
	(wt %)													(ppm)			
Jake_Matijevic																	
JM1	50.0	0.38	16.77	8.8	0.03	4.22	5.82	7.72	2.20	0.71	0.03	0.68	2.44	*nd*.	213	79	*nd*.
JM2 (nighttime)	49.7	0.64	14.75	11.2	0.21	4.07	6.53	6.51	1.95	0.61	0.04	0.78	2.83	58	360	112	*nd*.
Et_Then	46.5	0.37	8.84	25.5	0.40	4.05	3.88	3.22	1.50	0.89	0.04	0.56	3.81	273	389	*nd*.	*nd*.
Portage (soil)	45.6	1.08	9.92	18.8	0.43	7.54	6.50	2.58	0.57	0.73	0.38	0.55	5.10	455	363	37	*nd*.

[a]GUAPX is the fundamental parameters method of *Campbell et al*. [2012]. All analyses are of unbrushed rock surfaces, unless noted as a soil. Not detected = *nd*. See Figure 1 for location information.
[b]Total Fe is reported as FeO*.

Table 5. Statistical Error (2σ) of GUAPX[a] Results[b]

	SiO_2	TiO2	Al_2O_3	FeO*	MnO	MgO	CaO	Na_2O	K_2O	P_2O_5	Cr_2O_3	Cl	SO_3	Ni	Zn	Br	Ge
	(wt %)													(ppm)			
Jake_Matijevic																	
JM1	1.11	0.05	0.69	0.18	0.03	0.50	0.24	0.50	0.12	0.26	0.02	0.07	0.20	*nd.*	38	18	*nd.*
JM2 (nighttime)	1.2	0.09	0.46	0.2	0.04	0.23	0.23	0.32	0.12	0.12	0.03	0.07	0.19	52	50	22	*nd.*
Et_Then	1.5	0.14	0.55	0.6	0.10	0.43	0.28	0.52	0.18	0.26	0.07	0.11	0.37	260	160	*nd.*	*nd.*
Portage (soil)	1.1	0.10	0.37	0.3	0.05	0.31	0.20	0.21	0.06	0.11	0.05	0.05	0.22	90	54	19	*nd.*

[a]GUAPX is the fundamental parameters method of *Campbell et al*. [2012].
[b]Standard error is 2 sigma statistical. Not detected = *nd*.

although individual mineral grains could not otherwise be distinguished in images and this may reflect dust coverage and/or wind polish [*Minitti et al*., 2013]. Jake_Matijevic is interpreted to be float of likely volcanic origin.

4.1.2. Bathurst_Inlet

[21] Bathurst_Inlet is a gray, very fine-grained (silt size; <80 μm) rock (~35 cm high, ~40 cm long) with centimeter- to millimeter-scale laminations and a smooth, dusty surface (Figures 2c and 2d). The rock is angular with smooth fracture surfaces that suggest that it is coherent and well indurated. While the Bathurst_Inlet rock is a loose rock, it is surrounded by a dense field of blocks of similar albedo, angular morphology, and laminated texture that extend for several meters in all directions and is therefore thought to be representative of in-place (or only slightly moved) bedrock. Bathurst_Inlet is similar to Cowles, another rock target in the same area that was also examined by MAHLI [*Minitti et al*., 2013].

4.1.3. Rocks at Rocknest

[22] The Rocknest sand shadow, the subject of an extended scooping and SAM/CheMin campaign of an aeolian deposit, is on the western leeward side of a collection of loose low-albedo rocks with two contrasting morphologies: rough/vuggy and smooth/blocky/finely laminated. The two APXS targets, Et_Then and Rocknest_3, represent the two morphological types.

[23] Et_Then is a dark-toned, angular rock, ~6 cm across that was next to the rover's left front wheel during the scooping campaign (Figure 2e). Faceted edges and hollows suggest it is a ventifact. The rock's surface is extensively dust covered and pitted (possibly vuggy or vesicular). Parallel fractures cut across pits and are spaced ~1 cm apart. Dark gray to black, 1–3 mm long streaks that are visible in the MAHLI images are most likely areas where the dust cover is less—perhaps related to dust removal by saltating grains. The waxy sheen and dark coloration of the less dusty surfaces relative to other rocks may suggest the presence of a surface coating. The rock is partially buried and possibly recently exhumed from beneath the Rocknest sand shadow. It is apparently float, but it is morphologically similar to the collection of dark, vuggy rocks at the eastern end of the Rocknest sand shadow.

[24] Rocknest_3 is a dark, fine-grained, blocky rock (~30 cm long, ~6–8 cm high) with millimeter-scale laminations that are near horizontal but appear to be inclined at a very low angle in the upper half of the exposed rock face (Figure 2f). The rock has small circular voids throughout and ~1–2 cm long spindle-shaped voids that are spaced 3–10 cm apart and arranged along the lower part of the exposed rock face; these voids are thought to result from desiccation of finely laminated, fine-grained sediment [*Grotzinger et al*., 2013]. MAHLI did not image Rocknest_3 because of constraints imposed by physical management of Rocknest soil sample material cached inside the SA/SPaH. Microtextural information from Rocknest_3 was instead obtained from repeated ChemCam Remote Micro-Imager and LIBS observations. Grain size is at a scale smaller than the width of the ChemCam laser shot (~200 to 400 μm [*Tokar et al*., 2013]). The blocky, laminated morphology of Rocknest_3 links it to similar rocks at the western end of the sand shadow.

Table 6. Range and Average Minor and Trace Element Concentrations[a] of the Bradbury Assemblage by ChemCam PLS Analysis[b]

	# Points	Li	Rb	Sr	Ba
		(ppm)			
Jake_Matijevic					
Range	14	<5 – 40	20 - 60	*nd.* – 410	
Average		10	30	130	<100
Bathurst_Inlet					
Range	5	30 – 50	30 - 40	120 - 300	
Average		40	30	200	<200
Rocknest_3					
Range	38	<5 – 60	20 - 40	<50 – 250	
Average		10	30	100	<100
RMS error (±)		*40*	*30*	*170*	*640*

[a]*Ollila et al*. [2013b].
[b]Not detected = *nd*.

4.2. Dust Coverage and Surface Effects on APXS Analyses

[25] Rocks analyzed by the APXS exhibit varying amounts of dust/soil coverage. This coverage means that rock compositions contain contributions from both dust and the underlying rock. The amount of contamination by dust may be estimated using SO_3 contents (2.5–4.1 wt %; Table 2): i.e., dust has high S contents, but the rock itself is expected to be relatively S poor [e.g., *Yen et al*., 2005; *Blake et al*., 2013]. Consistent with this, Jake_Matijevic has the cleanest surface in MAHLI images and the lowest SO_3 of the rocks reported here (2.5 wt %). SO_3 contents suggest Rocknest_3 and Et_Then are similarly dusty (~4.1 wt %) and that Bathurst_Inlet has an intermediate dust cover. Chlorine correlates with sulfur in other Martian surface materials [e.g., *Gellert et al*., 2006], and Cl contents reported here are also likely in part contributed by surficial dust. In addition, the X-ray for the lightest elements detected by the APXS (Na, Mg, and Al) are largely contributed by the outer 2–3 μm of the target and thus dust coatings can block and/or contribute X-rays that combine with those from the underlying rock.

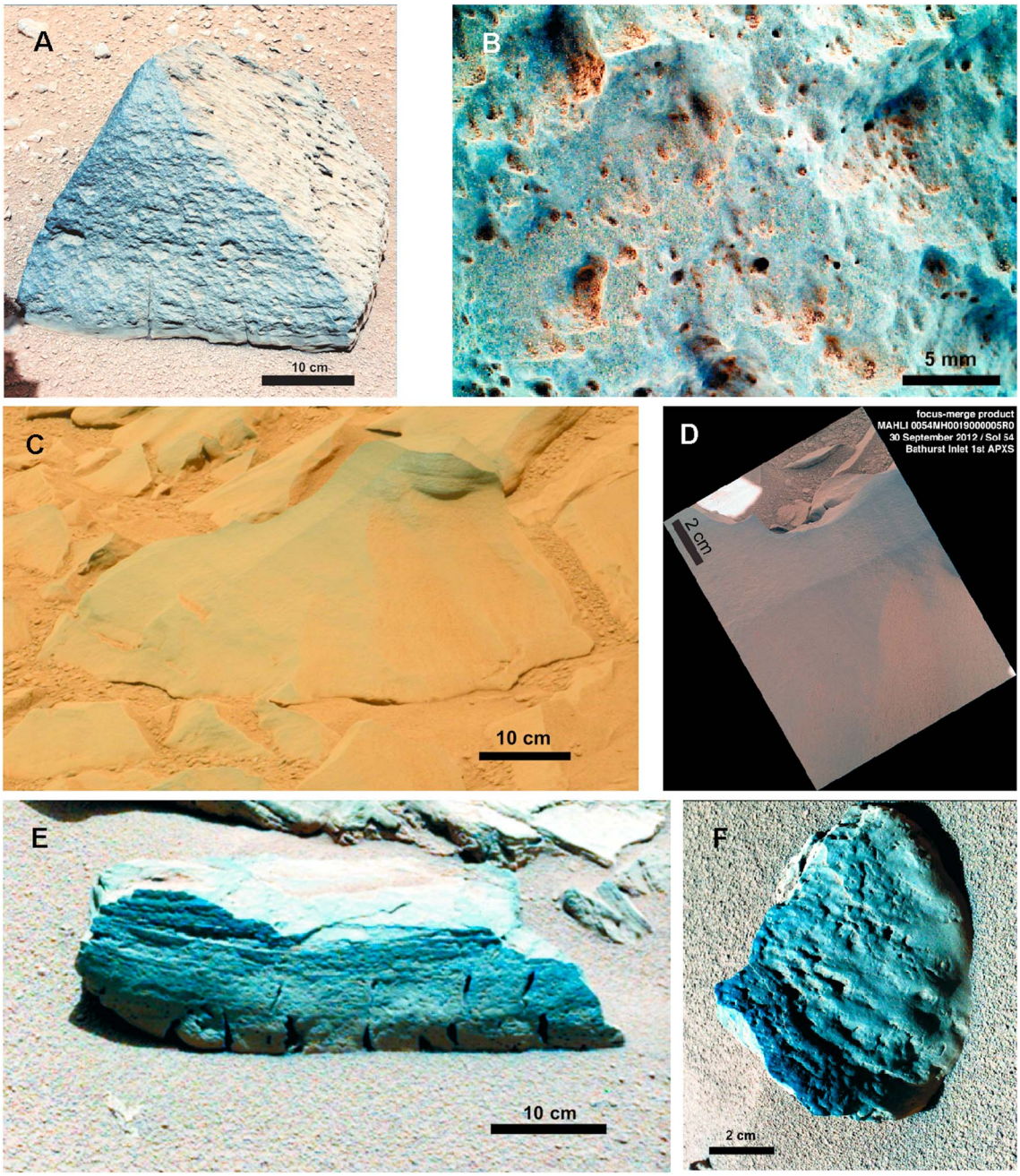

Figure 2. Images of Bradbury assemblage APXS rock targets. (a) Mastcam Left of Jake_Matijevic (#0046ML0212000000E1). (b) MAHLI image of Jake_Matijevic at 4.4 cm working distance (#0046MH0011001000E1). (c) Mastcam Right of Bathurst_Inlet, processed by the Mastcam team (original image #0053MR0245000000E1). (d) MAHLI of Bathurst_Inlet at 27 cm working distance, processed by the MAHLI team (original image #0054MH001900005RO). (e) MAHLI of Et_Then at 27 cm working distance (#0082MH009600100E1). (f) Mastcam Left of Rocknest_3 (#0059ML0269000000E1).

[26] To quantify the effects that increasing dust thickness covering a rock substrate has on APXS analysis, we use a new code devised by author Campbell for modeling X-ray yields from defined samples. The model requires input of rock substrate and dust cover composition, and we have chosen a terrestrial mugearite substrate from St. Helena [*Kawabata et al.*, 2011] and the Portage soil GUAPX concentrations (Table 4) to represent these. The actual composition of dust coatings on Martian rocks is likely to be different from Portage; we use it simply as an example of the kinds of effects that can be observed. Plots of the computed X-ray yields (i.e., the relative numbers of X-rays emerging from the two-layer sample in the direction of the X-ray detector) are presented in Figure 3. In reality, dust thicknesses are not constant, but if we regard the present results (Figure 3) as coming from successive values of mean thickness, these plots provide a sense of the uncertainties associated with unbrushed rock targets. At zero layer thickness, the yields are "pure" and

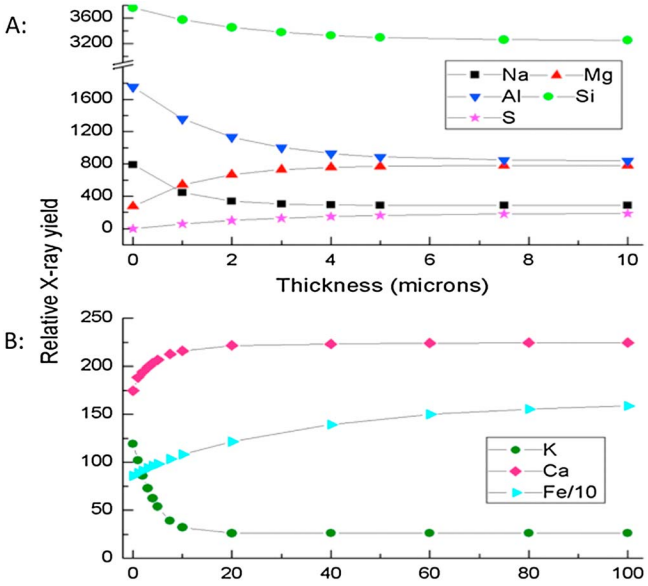

Figure 3. Relative X-ray yields calculated as a function of modeled Portage soil cover thickness on a St. Helena mugearite rock substrate [*Kawabata et al*., 2011] using the modeling code of Campbell. This code predicts the X-ray yields expected from a two-layer (dust on rock) target with given element concentrations in each layer and dust thickness. APXS yield provides essentially the reverse process to the spectrum analysis code GUAPX [*Campbell et al*., 2012], which is used for spectrum fitting and conversion of peak areas (X-ray yields) to concentrations. The calculations are subject to the same assumptions and approximations as the GUAPX code. X-ray yields are not adjusted to reflect detection efficiency or absorption in the Martian atmosphere, nor are the empirical correction factors discussed in *Campbell et al*. [2012] employed. For these reasons, and also because of the closure rule (that analyses must add to 100%), these results do not map directly to concentrations. (a) X-ray yields of the lighter elements (Na, Mg, Al, Si, and S) are compared to those of (b) the heavier elements K, Ca, and Fe.

solely derived from the mugearite. The light-element concentrations approach Portage soil concentrations (decreasing Na and Al and increasing Mg) as dust reaches ~2 µm thicknesses (Figure 3a). Yields for K and Ca with more penetrating PIXE-induced X-rays are shown in Figure 3b; about 10 µm of dust cover is now needed to complete the change from rock to Portage response. Finally, the iron signal is only slightly affected by a dust cover in the 1–10 µm range; the transition from the St. Helena mugearite signal to the full dust cover response requires thickness >100 µm; this is the case, indeed more so, for all heavier elements (e.g., Ni, Zn, and Br).

[27] These results suggest caution in drawing strong conclusions regarding the lighter elements (particularly Na, Mg, and Al) when there is a dust cover on the order of a few micrometers. To take an extreme example, the Na/Mg ratio for the example shown (Figure 3a) is inverted by just 3 µm of dust. We have deliberately chosen for illustrative purposes an example where the light-element concentrations of dust and substrate are very different, and in some combinations, (e.g., where the rock and dust compositions are more similar), the effects will be less dramatic. Without knowing surface layer thickness or rock composition, it is difficult to quantify the effects that dust coverage has on unbrushed rock surfaces. This problem is being addressed by ongoing and future studies [e.g., *Berger et al*., 2013].

[28] To correct for dust coverage, subsequent plots assume S- and Cl-free rock surfaces (renormalized to 100%) and, given the uncertainties involved, do not correct the light elements (Table 7). We acknowledge the limitations to this correction, particularly if the rocks themselves contain S or Cl or if the dust cover and rock are very different in light-element concentrations. In addition, we note that Martian magmas are relatively enriched in S and Cl relative to terrestrial ones [e.g., *Dreibus and Wänke*, 1985; *Filiberto and Treiman*, 2009; *McCubbin et al*., 2013; *Righter et al*., 2009]. Adjustments to whole-rock compositions made by this correction are relatively minor (factor of 1.04 to 1.1 increase).

4.3. APXS Results

[29] Compositions of the first four rocks and one soil examined by the APXS in Gale Crater as determined by the empirical (Gellert method) and fundamental parameter (GUAPX) approaches to reducing the spectra are presented in Tables 2 and 4, respectively. Figure 4 compares the compositions determined for the nighttime JM2 analysis by the two methods. Differences in concentration are mostly less than 10% for good quality nighttime spectra (cold temperatures and long durations), such as JM2, with the exception of certain elements (e.g., Mg and P), which are the subject of ongoing investigation. Differences in the results for the two lightest elements (Na and Mg) become larger for poorer quality daytime spectra (short durations and high temperatures), reflecting the increasing peak overlap caused by worsening energy resolution. The closeness of most concentrations for the long-duration, nighttime measurements validates the two methods when the energy resolution is good.

Table 7. APXS Concentrations of Bradbury Assemblage Rocks Recalculated Volatile-Free[a]

	SiO_2	TiO2	Al_2O_3	FeO*	MnO	MgO	CaO	Na_2O	K_2O	P_2O_5	Cr_2O_3	Ni	Zn	Br	Ge
	(wt%)											(ppm)			
Jake_Matijevic															
JM1	52.54	0.52	16.73	9.79	0.15	3.76	6.31	7.35	2.30	0.52	0.03	23	224	92	9
JM2 (daytime)	51.50	0.68	15.25	11.08	0.18	4.77	6.83	6.90	2.10	0.62	0.09	n.d.	356	99	4
JM2 (nighttime)	50.84	0.76	15.23	11.38	0.22	4.79	7.05	6.85	1.96	0.88	0.04	61	331	111	8
Bathurst_Inlet															
BI_For_Real	45.54	1.15	8.24	22.83	0.81	8.97	6.56	2.34	2.27	0.87	0.42	411	1385	15	85
BI_Top	45.87	1.09	8.39	21.76	0.45	9.17	6.72	2.24	3.01	0.93	0.37	334	1263	41	48
Et_Then	47.45	0.77	8.86	27.73	0.41	4.41	4.50	3.10	1.65	1.04	0.08	239	512	52	19
Rocknest_3	48.46	1.01	11.08	19.37	0.48	5.61	6.38	4.23	1.97	1.14	0.26	383	935	66	107

[a]Major and minor element oxide APXS compositions determined by Gellert method recalculated with 0% SO_3 and Cl and normalized to 100%.

[30] For the purposes of plotting the APXS results, we use the compositions determined by the Gellert method in order to better compare with the MER APXS data sets. We emphasize that neither method has been demonstrated to be more accurate than the other (although precision is well understood) and that our geological interpretations do not depend on which data set is used. Given the high degree of precision for both methods, variability outside the stated errors (Tables 3 and 5) between APXS targets on the same rock (e.g., MnO in Bathurst_Inlet) reflects heterogeneities in or at the surface of the rock, such as dust cover, proportions of mafic/felsic minerals, and/or mineral effects [*Campbell et al*., 2012].

[31] Previous missions have used APXS results to develop classification schemes by grouping similar rock types [e.g., *Squyres et al*., 2006]. However, the rocks reported on here are geochemically diverse and sufficiently distinct from one another to warrant each defining their own class. Given the clastic textures and degree of uncertainty about the geologic context for these rocks, igneous classification schemes should be considered as providing only general guidance about the compositions. Accordingly, we plot volatile-free Bradbury assemblage compositions on a total alkali versus silica diagram (Figure 5) such as has become common for relating different Martian rock compositions [e.g., *McSween et al*., 2009]. Soil contamination would probably pull the rock compositions in the general direction of the Portage soil with relatively low SiO_2 and total alkalis. Of the rocks examined, Jake_Matijevic is notably alkaline and evolved, plotting in the phonotephrite/tephriphonolite field in the total alkali versus silica diagram (Figure 5), but is classified as a mugearite because it is similar to terrestrial mugearites in most MgO and SiO_2 variation diagrams [*Stolper et al*., 2013]. The other three rocks are also alkali-rich with Bathurst_Inlet, Et_Then, and Rocknest_3 plotting within the basalt and hawaiite fields and near alkali-rich basalts found in Gusev Crater (Humboldt_Peak and Wishstone). Apart from the alkalis and certain trace elements, these three rocks are otherwise generally similar to the SNC meteorites, particularly in having high Fe and low Al contents.

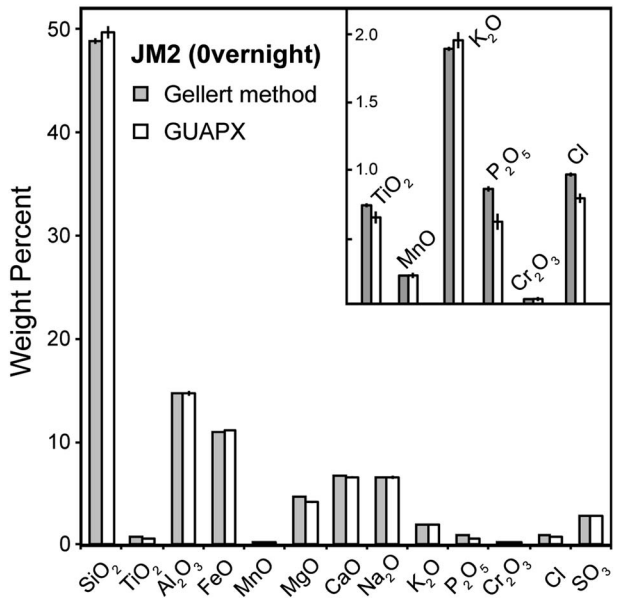

Figure 4. Bar graph comparing the APXS JM2 overnight elemental abundances in weight percent oxide as determined by the Gellert and GUAPX methods [*Gellert et al*., 2006; *Campbell et al*., 2012]. Statistical error bars are less than the width of the line where not visible. Inset graph presents minor element concentrations at a different scale.

[32] Although only four rocks were examined as of sol 102, the Bradbury assemblage spans nearly the entire Martian meteorite and mission data set in abundances of certain elements, particularly Fe and Mn. The MSL APXS measured the highest Fe (26.3 wt% FeO* in Et_Then) and Mn (0.78 wt% MnO in BI_For_Real) thus far measured by APXS for Martian basaltic rocks (Figure 6) with a range of 28 to 68 FeO*/MnO. CaO/Al_2O_3 ratios of the Bradbury assemblage are subchondritic and are in this respect like most Gusev rocks, but the Bradbury rocks cover the whole range of Al_2O_3 found in relatively unaltered Gusev basalts (Adirondack, Backstay, Irvine, and Humboldt Peak; Figure 6b).

[33] While diverse in many respects, the Bradbury assemblage rocks also share certain characteristics, in particular high abundances of potassium (1.6–2.9 wt%; Figure 6c). Moderately volatile metals (Zn and Ge) are also high in some targets; 1210 to 1330 ppm Zn is found among the Bathurst_Inlet targets (Figures 6d and 7c), and 102 ppm Ge is found in Rocknest_3 (Table 2). Concentrations of K and Zn do not correlate with halogen or S contents, as illustrated in a plot of K_2O versus Cl (Figure 6e), suggesting that these moderately volatile metals are not associated with salts, in contrast to some rock analyses from other landing sites (e.g., Mazatzal [*Squyres et al*., 2004b; *Morris et al*., 2008]). Individual rocks from the Home Plate region of Gusev Crater region that are similarly enriched in K and Zn (e.g., FuzzySmith and Montalva [*Ming et al*., 2008]) show

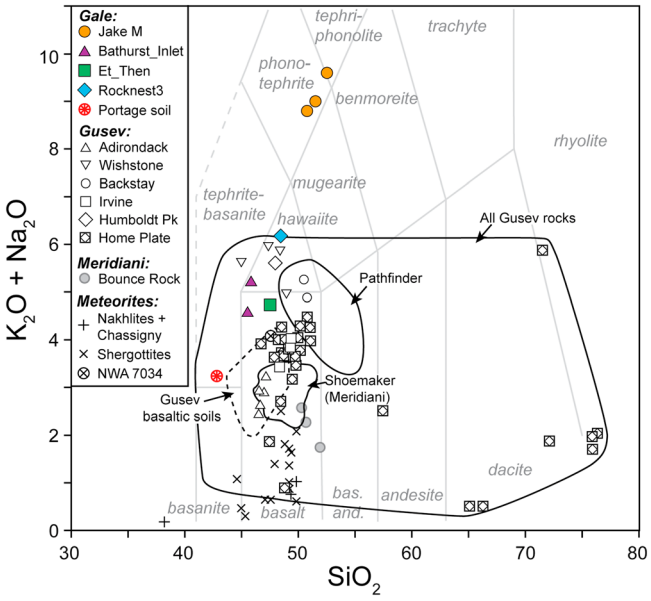

Figure 5. Total alkali versus silica diagram with igneous classification scheme after *Le Bas et al.* [1986]. Compositions of Martian rocks (volatile-free) determined by APXS plotted include the first four rocks and Portage soil in Gale crater, the relatively unaltered basalts and hydrothermally altered Home Plate rocks from Gusev crater, the Shoemaker formation and Bounce Rock from Meridiani Planum, and the Pathfinder rocks [*Ming et al.*, 2008; *Gellert et al.*, 2006; *Brückner et al.*, 2003; *Squyres et al.*, 2012; *Zipfel et al.*, 2011]. The Martian SNC meteorites are also shown [*Meyer*, 2013; *Agee et al.*, 2013]. The 2σ standard errors (Table 3) are generally smaller than the symbols.

evidence of being hydrothermally altered; FuzzySmith has high SiO_2 concentrations and Mössbauer spectrometer observations suggest that it likely contains marcasite or pyrite, and Montalva has very high Fe^{3+}/Fe_T (0.93 [*Morris et al.*, 2008]).

[34] The rock Jake_Matijevic is the most likely igneous rock examined so far in Gale Crater, and its chemistry and a potential scenario for its petrogenesis are described in detail by *Stolper et al.* [2013]. Jake_Matijevic is more fractionated than most known Martian igneous rocks, having low Mg and Mg# of 44.6–47.4 (Mg# is molar MgO/(FeO + MgO) × 100; assuming $Fe^{3+}/Fe_{Total} = 0.15$). Its Ni and Cr contents are also low (below detection to 59 ppm Ni and 225–583 ppm Cr; Figure 7d); the Ni is, in fact, the lowest found to date for an unbrushed rock target on the surface of Mars. The high Na_2O concentrations (6.6–7.1 wt%) of Jake_Matijevic are also remarkable relative to other Martian compositions, particularly given its dusty surface. The high alumina and alkali concentrations make Jake_Matijevic a truly alkaline composition rock with 16% normative nepheline (assuming $Fe^{3+}/Fe_T = 0.15$; Figure 8 and Table 8).

[35] In contrast, Bathurst_Inlet is more mafic and is much richer in Fe (20.8–21.9 wt% FeO*) than Jake_Matijevic. Bathurst_Inlet ranges to the highest K_2O of the Bradbury assemblage, and it is relatively Al poor (7.9–8.0 wt% Al_2O_3) and slightly hypersthene normative (Figure 8 and Table 8). There is uncertainty as to whether Bathurst_Inlet represents an igneous composition, but even if so, its relatively low Mg# (45.2–46.9) and silica saturation with respect to normative mineralogy indicate that it could not be parental to Jake_Matijevic by fractional crystallization at low pressures. Slightly higher FeO* found in the BI_For_Real than in BI_Top correlates with higher concentrations of transition metals (beyond stated errors), including Ti, Cr, Ni, Zn, and especially Mn (Figures 6b and 7d). These elements are compatible in oxide minerals, such as magnetite, and may suggest one of these is present in this rock.

[36] Rocknest_3 is intermediate in composition between Jake_Matijevic and Bathurst_Inlet in most variation diagrams (Figures 6 and 7). Although not as extreme as Jake_Matijevic, Rocknest_3 is silica undersaturated with ~3% normative nepheline (Figure 8). In most element-element variation diagrams as well as in a plot of Al/Si versus (Fe + Mg)/Si, Rocknest_3 plots along a line joining Jake_Matijevic and Bathurst Inlet, suggestive of a two-component mixing relationship (Figures 6 and 7) that likely reflects mechanical mixing by sediment transport. Exceptions from the mixing trend include Cl, P, Ni, Ge, and MgO versus FeO (Figure 7b) and may imply that multiple processes (e.g., dust coverage effects on light-element concentrations or dissolution of olivine or other mineral phases) have contributed to the Rocknest_3 composition.

[37] The float rock Et_Then is distinct from the other rocks examined by the APXS, having very high FeO* (26.3 wt%) and low MgO (4.2 wt%) contents (Mg# = 25; Figure 7b). The high FeO* in Et_Then does not correlate with elevated Mn, Ti, or Cr, in contrast to Bathurst_Inlet. Et_Then is the only rock of the Bradbury assemblage that is strongly hypersthene normative (22%; Figure 8), although we note that the high Fe with low Mn and Ti are likely not reflective of an igneous bulk composition. More probably, aqueous alteration involving the addition of Fe contributed to the Et_Then composition.

[38] In order to evaluate the relative proportions of primary phases in the Bradbury assemblage rocks, we plot molar proportions of FeO* + MgO, Al_2O_3, and CaO + Na2O + K2O on a ternary diagram (Figure 9). Felsic and mafic igneous minerals plot at distinct locations on this diagram. The position of Jake_Matijevic is consistent with a composition that is relatively enriched in aluminosilicate minerals, while Bathurst is consistent with a composition that is more enriched in ferromagnesian minerals. Rocknest_3 plots at an intermediate position and supports the suggested mixing relationships.

[39] Figure 9 is also useful for examining the effects of moderate pH subaerial weathering [*Nesbitt and Wilson*, 1992]: as igneous minerals are chemically weathered, they tend to lose soluble cations (Na, K, Ca, and Mg) in preference to less soluble cations (Al and ferric iron), causing progressive enrichment in Al and Fe, evolving on a trend perpendicular to the tie line between feldspar and the FeO* + MgO apex. Previous in situ and experimental studies have thus used this diagram to distinguish between terrestrial and Martian-style chemical weathering, which is dominated by olivine dissolution processes [e.g., *Hurowitz et al.*, 2006]. By this approach, the Bradbury assemblage rocks do not display any noticeable terrestrial weathering trend. Chemical or diagenetic processes such as olivine dissolution or the addition of Fe (or Mn-rich) oxides as a coating or cement would lead to trends away from or toward the FeO* + MgO apex and are consistent with observed

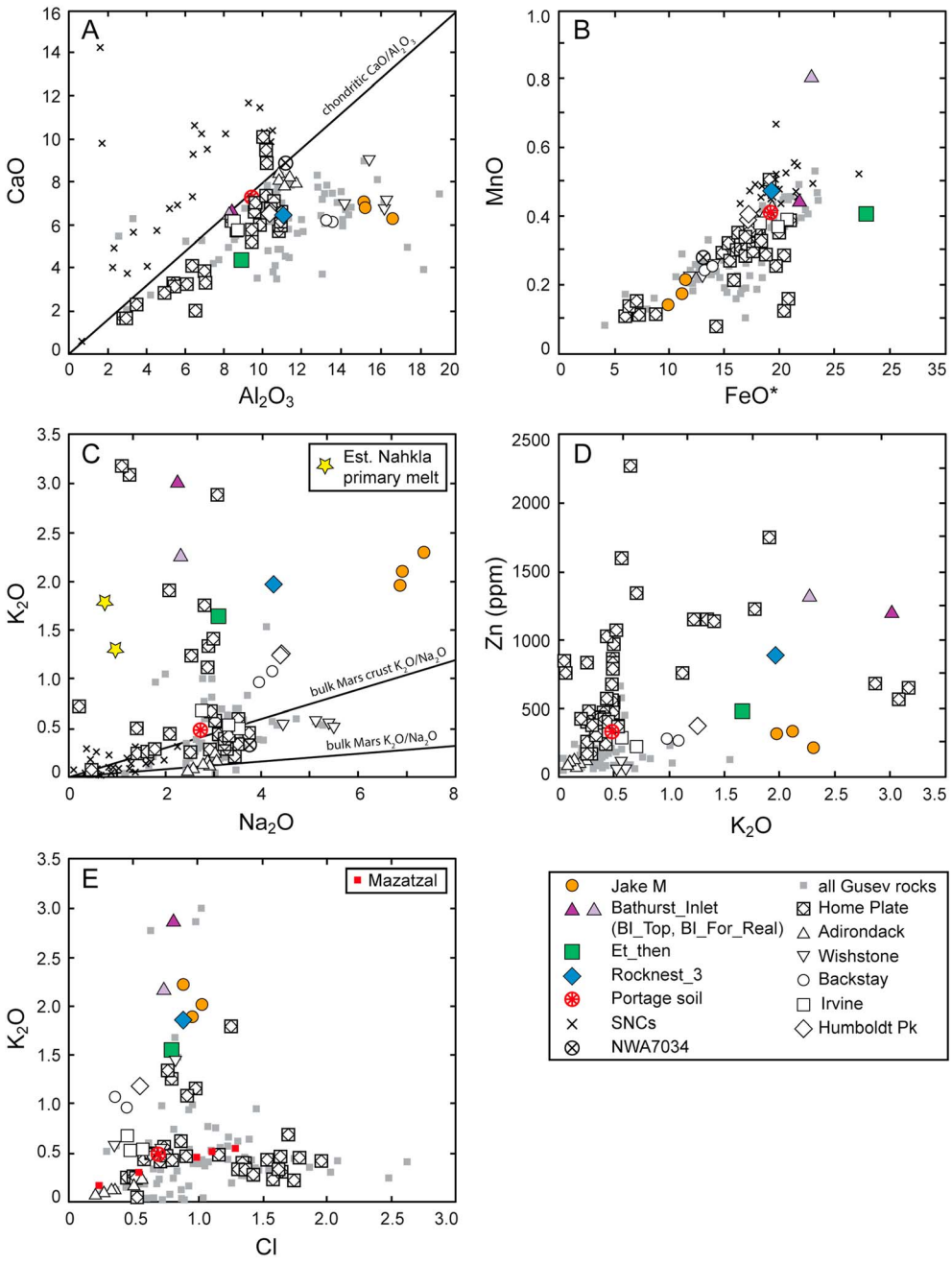

Figure 6. Geochemical variation diagrams for Martian rock compositions, including the Martian SNC meteorites and rock compositions determined by APXS from Gale crater (Jake_Matijevic, Bathurst, Et_Then, and Rocknest_3) and Gusev crater (Home Plate, Adirondack, Wishstone, Backstay, Irvine, and Humboldt Peak). The Portage soil from Gale Crater represents the Mars global soil [*Blake et al*., 2013]. Compositions are plotted as weight percent and assumed to be volatile-free, except where noted. (a) A plot of CaO versus Al_2O_3 with line denoting the chondritic ratio of CaO/Al_2O_3 [*Sun and McDonough*, 1989]. (b) MnO versus total Fe as FeO*. (c) K_2O versus Na_2O. Estimated Nahkla primary melt compositions are from *Goodrich et al*. [2012, 2013]. Estimated bulk Mars and bulk Mars crust compositions are from [*Wänke and Dreibus*, 1988] and [*Taylor and McLennan*, 2009], respectively. (d) Zn versus K_2O. (e) Plot of K_2O versus Cl (not volatile-free) includes the Adirondack class rock Mazatzal, whose KCl-rich rind was progressively abraded by the Rock Abrasion Tool [*Ming et al*., 2008; *Gellert et al*., 2006; *Brückner et al*., 2003; *Squyres et al*., 2012; *Zipfel et al*., 2011; *Meyer*, 2013; *Agee et al*., 2013].

variations. Because compositions of the Bradbury assemblage can be interpreted as being essentially mixtures of igneous minerals, these rocks are interpreted to be of volcanic/volcaniclastic origin with little subsequent leaching of soluble cations by water, or if they are sedimentary rocks, their sources underwent at most only incipient subaerial weathering with little attendant modification of primary bulk igneous compositions [*McLennan et al*., 2013].

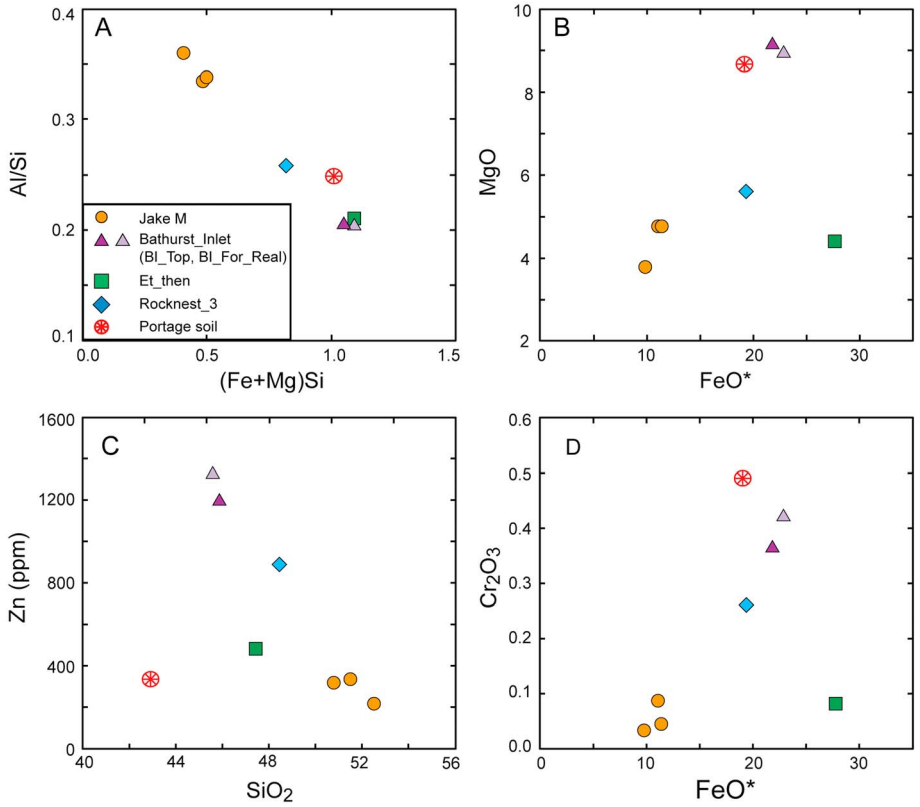

Figure 7. Geochemical variation diagrams for the Bradbury assemblage and Portage soil determined by APXS. Concentrations are in weight percent, unless noted. (a) Al/Si versus (Fe + Mg)/Si. (b) MgO versus FeO*. (c) Zn versus SiO_2. (d) Cr_2O_3 versus FeO*.

4.4. ChemCam Results

4.4.1. PLS Analysis

[40] ChemCam analyses of the rocks in the HP unit, including Jake_Matijevic, are variable depending on location, indicating that all of the rocks encountered in this region are medium (>100 μm) or coarse grained (>400 μm), heterogeneous, and composed of a mixture of felsic and nonfelsic minerals [*Stolper et al.*, 2013]. Compositions of Bathurst_Inlet and the rocks around Rocknest (LF unit) are less variable, indicating these lithologies are more fine-grained and homogeneous. (ChemCam did not analyze Et_Then due to its close proximity to the rover.) More than 50 observation points by ChemCam on Jake_Matijevic, Bathurst_Inlet, and Rocknest_3 confirm the near linear mixing trend observed in APXS analyses.

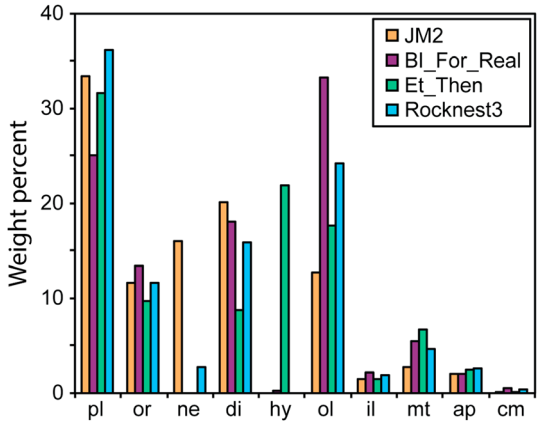

Figure 8. Bar graph portraying the CIPW normative mineral contents in weight percent of representative Bradbury assemblage APXS analyses. (pl = plagioclase, or = orthoclase, ne = nepheline, di = diopside, hy = hypersthene, ol = olivine, il = ilmenite, mt = magnetite, ap = apatite, and cm = chromite).

[41] A detailed investigation of the rocks around Rocknest found that the variations in texture (rough versus smooth/blocky/laminated) do not correlate to variations in composition. Unlike the differences in Fe contents observed between Rocknest_3 and Et_Then by the APXS (Figure 6b), the Fe contents of other rough-textured rocks were not significantly elevated over the range observed over 38 different Rocknest_3 measurements. In addition, the location-to-location variability within individual rocks is similar to variability observed between the different rocks, some of which have high iron contents similar to Et_Then.

[42] ChemCam can also yield insight to the variability observed among minor elements in the APXS rock targets (Table 6). In particular, MnO is variable among the two Bathurst_Inlet APXS targets (0.43–0.78 wt %). Estimated Mn abundances over the five ChemCam locations indicate a broad consistency between the two instruments, with ChemCam abundances near the BI_For_Real APXS measurement. There are minor variations in Mn between locations but no significant change in depth over each 30-shot depth profile. Cr observations from ChemCam follow the trends seen in the APXS data with relative

Table 8. CIPW Normative Mineralogy of the Bradbury Assemblage[a]

	Jake_Matijevic (JM2) [c]		BI_For_Real		ET_Then		Rocknest_3	
Fe^{3+}/Fe_{total} [b]	0.15	0.25	0.15	0.25	0.15	0.25	0.15	0.25
Plagioclase	33.4	34.9	25.1	25.1	31.6	31.6	36.1	38.8
Orthoclase	11.6	11.6	13.4	13.4	9.8	9.8	11.6	11.6
Nepheline	16.0	15.2					2.8	1.3
Diopside	20.2	20.0	18.1	18.1	8.7	8.7	15.9	15.8
Hypersthene			0.2	0.2	22.0	28.8		
Olivine	12.7	10.5	33.3	33.2	17.7	6.8	24.3	20.3
Ilmenite	1.4	1.4	2.2	2.2	1.5	1.5	1.9	1.9
Magnetite	2.8	4.6	5.5	5.5	6.7	11.2	4.7	7.8
Apatite	2.0	2.0	2.0	2.0	2.4	2.4	2.6	2.6
Chromite	0.1	0.1	0.6	0.6	0.1	0.1	0.4	0.4
$100 \times Mg/(Mg + Fe^{2+})$ in rock	47	50	45	48	25	27	38	41
$100 \times Mg/(Mg + Fe^{2+})$ in silicates	51	56	48	54	27	32	41	46.
$100 \times Ca/(Ca + Na)$ in rock	36	36	61	61	45	45	46	46
Plagioclase An content	14	14	20	20	16	16	14	13

[a]CIPW norm calculations were determined using APXS compositions by the Gellert method (Table 2).
[b]Fe^{3+}/Fe_{total} reflects the range determined in relatively unaltered basalts analyzed by Mössbauer spectrometer in Gusev Crater [*Morris et al*., 2008; *Schmidt et al*., 2013].
[c]Calculation done using the JM2 nighttime analysis.

increases in abundance from Jake_Matijevic to Rocknest_3 to Bathurst_Inlet (as in Figure 7d).

[43] Trace elements detected by ChemCam and not reported by APXS include the alkali elements Li and Rb and the alkaline earth elements Sr and Ba (Table 6). Concentrations of Li are <10 ppm for most spots on Jake_Matijevic and Rocknest_3 but range at 40 to 60 ppm for individual spots on the two rocks. All five analyzed spots on Bathurst_Inlet have Li > 30 ppm (30–50 ppm), but decreasing Li abundance with depth (30 individual shots) may indicate that the exterior has been altered by chemical weathering [*Ollila et al*., 2013b; *Lanza et al*., 2013]. Jake_Matijevic has the most shot-to-shot variability in Rb and Sr, ranging from 20 to 60 ppm Rb and from below detection to ~400 ppm Sr; this is consistent with these elements being concentrated in phases, such as plagioclase or alkali feldspar. Rb is more homogeneously distributed in the K-rich Bathurst_Inlet (30–40 ppm). Ba is a difficult element to determine with ChemCam spectra due to several interfering peaks [*Ollila et al*., 2013b]; close examination of the spectra indicates that Ba is present at most analyzed spots on these rocks but at a level that is difficult to quantify (although <200 ppm; RMS error ±640 ppm).

4.4.2. Alkali Variability by ICA Analysis

[44] All rocks, gravels, and pebbles analyzed by the ChemCam instrument along the Curiosity traverse during the first 90 sols were classified using independent component analysis (ICA [*Forni et al*., 2013]). This method, which allows classification of the wide range of peaks characterizing a LIBS emission spectrum, reveals variability in elemental concentrations among ChemCam targets. In a K-Na ICA plot (Figure 10), two regions can be distinguished. The first is circled in yellow and includes Jake_Matijevic (JM1 to JM14) and all float rocks, gravels, and coarse soils [*Meslin et al*., 2013] analyzed by the ChemCam instrument from sol 13 to 50 (i.e., from sites at or near Bradbury Landing and up to just before Rocknest). It is characterized by high Na relative to K but with a large degree of point-to-point variability. The second region is circled in blue and

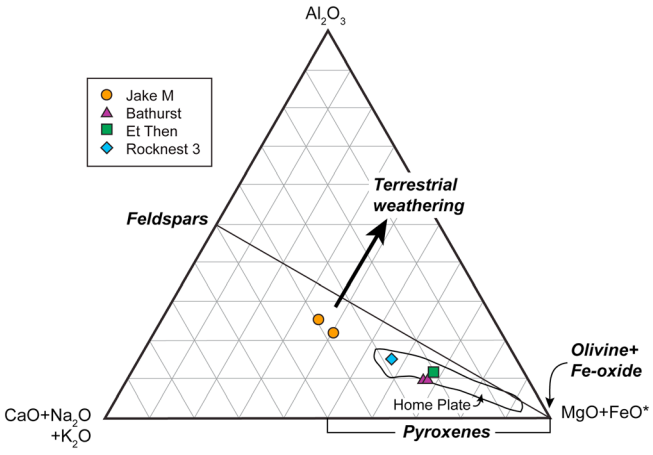

Figure 9. Ternary diagram representing the molar proportions of Al_2O_3, $CaO + Na_2O + K_2O$, and $MgO + FeO^*$ of the Bradbury assemblage. The important mineral (feldspar, pyroxene, olivine, and Fe oxide) groups and the direction that terrestrial weathering pulls compositions are indicated for reference. See text for discussion. The field for Home Plate (Gusev) includes all basaltic layered rocks in the vicinity of the Home Plate outcrop. Data are from *Ming et al*. [2008] and the Planetary Data System.

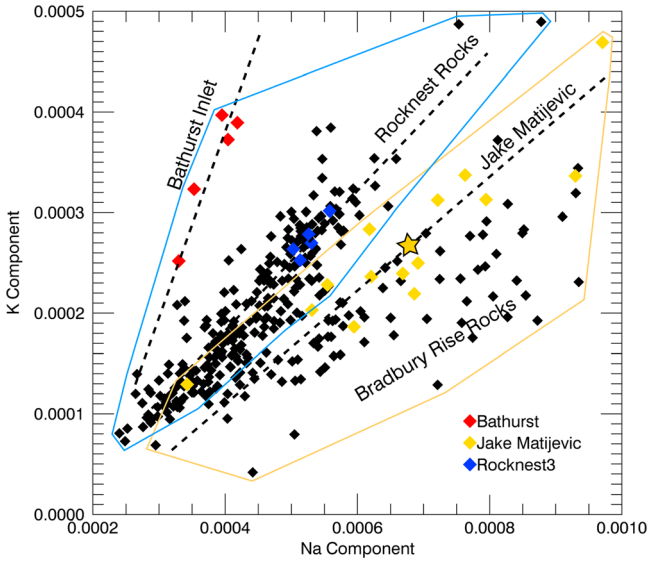

Figure 10. Plot of K versus Na components by ChemCam independent component analysis (ICA) for rock targets to sol 100. Colored symbols represent ChemCam analyses for the APXS targets. The yellow star is average Jake_Matijevic. Black symbols are all other rock targets examined by ChemCam along the rover's traverse to sol 100. The fields are discussed in the text.

comprises rocks examined by ChemCam after sol 50 and includes the APXS targets Bathurst_Inlet and Rocknest_3. These targets have higher K relative to Na, with Bathurst_Inlet being the most K-rich. Although there is a great deal of variability shot to shot, the ChemCam data are in qualitative agreement with variations seen among the APXS data (Figure 6c).

[45] Considering all the ChemCam points in detail (14 for Jake_Matijevic, 38 for Rocknest_3, and 5 for Bathurst_Inlet), the three rocks define three distinct K/Na trends. Each trend is interpreted to represent mixing between ferromagnesian (Na, K-poor) and felsic (Na-K-rich) compositions (likely alkali feldspar). In comparison, all Rocknest rock points plot along a line of higher K/Na and Bathurst_Inlet has even higher K/Na relative to Jake_Matijevic. One exception to these trends is the pebble conglomerate Link [*Williams et al*., 2013], which has more variable K/Na than the other rock targets and suggests mixing of Na-rich and K-rich components.

5. Discussion

[46] With only four rocks analyzed by the APXS so far in Gale Crater and uncertainty as to their geologic context (e.g., outcrop versus float and geologic origin), additional analyses would be desired to fully understand the Gale landing site. Nonetheless, the K- and Fe-rich compositions are intriguing, and the following section discusses their possible origins. We also discuss implications for understanding the geology of Gale Crater and the range of rock compositions on Mars.

5.1. Rock Origins

[47] Although only one rock (Jake_Matijevic) is convincingly igneous (largely on compositional grounds [*Stolper et al*., 2013]), two other Bradbury assemblage rocks Rocknest_3 and Bathurst_Inlet have igneous-like bulk compositions with reasonable CIPW normative mineralogies that are consistent with those of terrestrial igneous rocks and Martian meteorites (Table 8). The high-Fe rock Et_Then is not considered igneous and is discussed later in this section. Unlike most igneous rock suites on Earth, whole-rock compositions determined by APXS do not indicate decreasing Mg# with increasing SiO_2; additionally, their CIPW normative mineralogies are on both sides of the critical plane of silica saturation. These observations indicate that the four rocks of the Bradbury assemblage cannot be linked by fractional crystallization at low pressure. High-pressure fractional crystallization has been suggested to generate Jake_Matijevic and other Martian alkaline magmas [*Stolper et al*., 2013; *Whitaker et al*., 2007], and this process can lead to increasing alkalis and decreasing Mg# with constant or decreasing SiO_2. We, however, note that other Bradbury compositions do not fall along fractional crystallization trends modeled for Jake_Matijevic by *Stolper et al*. [2013] or for other terrestrial alkaline suites [e.g., *Nekvasil et al*., 2004; *Frost and Frost*, 2008] but that future experiments may demonstrate an igneous fractionation relationship between these magmas.

[48] Instead, mixing between Jake_Matijevic-like and Bathurst_Inlet-like materials more likely explains why Rocknest_3 plots between these targets in almost all variation diagrams. The laminated texture of Rocknest_3 makes it the most clearly sedimentary of the Bradbury assemblage, and the fine grain size could reflect transport over a relatively large distance. Thus, mixing of two (or more) components as suggested by geochemical variations is plausible and could reflect tapping of different source areas. Rocknest_3 bulk composition (APXS) is consistent with ~44% Jake_Matijevic-like materials and ~56% Bathurst-Inlet-like materials (±12% for uncorrected concentrations, except where noted; Table 2). The exceptions are Mg, S, Cl, P, and Ni (Figures 6e and 7b). Surface dust cover may strongly influence Mg, S, Cl, and Ni (i.e., dust is enriched in S, Cl and Ni, and dust masks light-element concentrations determined by APXS in the underlying rock [*Yen et al*., 2005]). Dissolution of olivine at the rock surface may also affect Mg and Ni concentrations [*Hurowitz et al*., 2006]. Alternatively, imperfect mixing may indicate different sedimentary processes and/or source contributions.

[49] When first encountered, Jake_Matijevic was interpreted as an exotic block, perhaps ejected to its current position by an impact outside Gale Crater. Its high K and apparent mixing relationship with Bathurst_Inlet and Rocknest_3 suggests, however, that Jake_Matijevic may be more locally derived and (or) represent a larger block of the sediment source material that contributed gravels and clasts to Bradbury Rise. This component is Na- and Al-rich and Fe- and Cr-poor (Figures 5 and 6). ChemCam shots of pebbles in soils and conglomerates have high Na and Al contents and may also represent Jake M-like material (Figure 10; *Sautter et al.* [2014]). By analogy with similar terrestrial rocks, the igneous processes necessary to produce the composition of Jake_Matijevic could involve partial melting of a water-rich metasomatized Martian mantle followed by fractional crystallization at depth [*Stolper et al*., 2013].

[50] The Fe-, Mg-, and Zn-rich and Si- and Al-poor Bathurst_Inlet may also represent an important component of the local rocks and sediments. So far, only one rock-like

Bathurst_Inlet has been examined by Curiosity, but mapping suggests that Bathurst_Inlet may be part of a more extensive unit on the eastern flank of Bradbury Rise [*Sumner et al*., 2013]. The layered structure, fine grain size (300–500 μm), and apparent lack of primary igneous textures of Bathurst_Inlet suggest a sedimentary or volcaniclastic origin involving transport prior to deposition and lithification. The composition of Bathurst_Inlet is unusual with high K and Zn relative to the bulk Martian crust (e.g., 2.9 wt % versus 0.45 wt % K_2O and up to 1330 versus 320 ppm Zn [*Taylor and McLennan*, 2009]) and suggests a limited degree of mixing with other lithologies during transport. The absence of any Al enrichment along a typical terrestrial weathering trend (Figure 9) further suggests limited weathering or alteration of igneous mineralogy, although addition of Fe oxides is also consistent. Enrichments in moderately volatile metals may indicate interaction with a hydrothermal fluid, either in the source region or at the site of deposition such as has been suggested for the altered basaltic tephra deposits of Home Plate in Gusev Crater [e.g., *Schmidt et al*., 2009]. We note that Home Plate also does not present a terrestrial-style weathering trend in Figure 9. ChemCam analysis of Bathurst_Inlet suggests elevated Li at the rock surface, which may be consistent with low-level aqueous alteration that resulted in fluid-mobile Li to be leached from the interior and concentrated at the surface [*Ollila et al*., 2013b].

[51] High concentrations of Fe are a characteristic shared by the Bathurst_Inlet, Rocknest_3, and Et_Then targets. For Bathurst_Inlet and Rocknest_3, Fe contents correlate with high abundances of Mg as well as compatible transition metals (Mn, Zn, Ti, Ni, and Cr). This observation is consistent with the presence of olivine, pyroxene, and possibly magnetite and chromite in these rocks. High and variable Mn contents in Bathurst_Inlet (Figure 6b) also suggests redox reactions in the presence of aqueous fluids during weathering at the Martian surface [e.g., *Morford and Emerson*, 1999]. Et_Then, however, differs in that it has the highest Fe of all the rocks we studied (Figure 6), while also having low Mg and Cr concentrations (Figure 7). In addition, it has high FeO/MnO (67.5). High FeO/MnO correlates with Fe^{3+}/Fe_{Total} at the MER landing sites based on Mössbauer spectroscopy [e.g., *Rieder et al*., 2004]. These observations may be consistent with Et_Then containing hematite and/or other Fe^{3+}-bearing oxides that precipitated from aqueous fluids, as pore-filling cements [e.g., *Chan et al*., 2000; *Walker et al*., 1981] or as a rind near the outer surface of the rock following dissolution of more soluble cations and reprecipitation of oxidized Fe [e.g., *Dixon et al*., 2002].

5.2. Contribution to Understanding the Geology of Gale Crater

[52] Exploration of Gale Crater is ongoing, and there are many unanswered questions about the Bradbury assemblage. These include the following: What is their extent beyond Bradbury Rise? How do these rocks compare to the overall diversity of rocks that are still to be encountered in Gale Crater? And does the ultimate source of these rocks lie inside or outside Gale Crater?

[53] An association between the Bradbury rocks and nearby fluvial conglomerates [*Williams et al*., 2013] is suggested by their compositional similarity to Jake_Matijevic as determined by ChemCam (Figure 10). These rocks may have been transported from a common source region, perhaps as far distant as the rim of Gale Crater and carried to the landing site area via the Peace Vallis alluvial fan network. The unusual alkali-rich compositions that are unlike the average composition of the Martian crust [e.g., *Taylor and McLennan*, 2009], however, suggest that mixing during transport only involved alkaline compositions and is consistent with more localized source, possibly from within Gale Crater. Alternatively, transport via impact processes or volcanic flows (e.g., pyroclastic flows) are possible.

[54] To test models of rock provenance, we will need to track the distribution of different rock types along Curiosity's ~8 km traverse from Yellowknife Bay to Mt. Sharp. Lobes of the fan system may be mappable by the range in clast lithologies to support a distant source. Alternatively, the rover might encounter in-place lavas or volcanic deposits of similar composition to one of the Bradbury assemblage rocks that would suggest a more local volcanic source.

5.3. Origin of K_2O-Rich Melt and Implications for Differentiation of the Martian Mantle

[55] The recognition that the Bradbury assemblage is enriched in alkalis, especially potassium, raises the question of what source compositions or igneous processes might generate such rocks (or their magmatic precursors). Although the composition of Jake_Matijevic most likely represents a magma [*Stolper et al*., 2013], it is not so clear that the other three Bradbury rocks are igneous or if their high-K contents can be attributed to magmatic processes. Here, we assume that because all four of the Bradbury assemblage rocks are enriched in alkalis and because one is likely igneous, the characteristics of all reflect an igneous parentage.

[56] Mars might be expected to generate magmas that are on average richer in alkalis than the Earth because geochemical models predict that Mars's mantle (on average) has higher average abundances of alkalis and other moderately volatile elements than does the Earth's mantle [e.g., *Wänke and Dreibus*, 1988]. However, it is not clear how alkalis (especially K) might become as enriched as observed in the Bradbury assemblage. End-member igneous events that might reasonably affect the evolution of Martian magmas include the following: (1) low-volume partial melting of normal Martian mantle [*Wänke and Dreibus*, 1988], (2) fractional crystallization of known Martian primary melts, (3) crustal assimilation of basaltic crust, and (4) a regional characteristic inherited from mantle sources underlying Gale.

[57] The first three events are ruled out by simple petrologic models. To generate the average K_2O concentration of Bathurst_Inlet by simple batch partial melting of normal Martian mantle (0.03 wt% K [*Wänke and Dreibus*, 1988]), very low-degree melting of less than 2% is required (bulk K partition coefficient of 0.002 [*Schmidt and McCoy*, 2010]). Such melt fractions are insufficient to allow significant melt migration to occur [e.g., *Schmeling*, 2000]. Fractional crystallization was examined by *Stolper et al*. [2013] for the generation of Jake_Matijevic, although they note that fractional crystallization of any known Martian primary melts will not generate the alkali contents of Jake_Matijevic under any condition. In addition, back-of-the-envelope Rayleigh fractional crystallization calculations require >95% crystallization of Adirondack-like basalt (Gusev Crater [*Gellert et al*., 2006]) to reach the elevated K concentrations of average

Bathurst_Inlet. This high degree of crystallization is inconsistent with its major element compositions and especially with its elevated abundances of igneous compatible elements (Ni and Cr). Assimilation of basaltic crust by mantle-derived basaltic magmas is also unlikely because partial melts of basaltic lithologies are too rich in SiO_2 at crustal depths (>65% [e.g., *Beard and Lofgren*, 1991]) to play a significant role in the generation of Si-poor, alkali-rich compositions like Jake_Matijevic or Bathurst_Inlet by mass balance [e.g., *Schmidt and McCoy*, 2010].

[58] Having ruled out simple igneous processes, we can make inferences about character of a regional mantle component that could contribute high alkalis such as in the Bradbury assemblage. An enriched mantle source has been invoked for the geneses of various Martian meteorite magmas [e.g., *Treiman*, 2003; *Jones*, 2003; *Borg and Draper*, 2003; *Debaille et al*., 2008] and for some Gusev basalts [e.g., *Schmidt and McCoy*, 2010; *Usui et al*., 2008]. The mantle component that contributed to Bradbury assemblage must be relatively poor in Na to yield high K/Na relative to the bulk Martian crust (K/Na = 0.09 [*Taylor and McLennan*, 2009]), such as is observed in Bathurst_Inlet (K/Na = 1.1 to 1.5; Figure 6c).

[59] There is general consensus that Mars had a magma ocean early in its history [e.g., *Mezger et al*., 2013], and the shergottite Martian meteorites show radiogenic isotopic characteristics consistent with the late fractionate of that ocean [e.g., *Debaille et al*., 2009]. Magma ocean processes involving a significant fraction of plagioclase, the major mineralogic host of Na, or of sodic clinopyroxene could increase K/Na. One hypothesis is that the Martian magma ocean had a K-rare earth element (REE)-enriched final melt fraction: so-called "Martian KREEP component" [*Treiman*, 2003] This component must have had K_2O/Na_2O >0.2, like the potassium, rare earth element, and phosphorus (KREEP)-richest meteorites (those with the highest Na_2O [*Debaille et al*., 2009]), similar to that of bulk Mars [e.g., *Lodders and Fegley*, 1997; *Halliday et al*., 2001] because plagioclase crystallizes very late in a Martian magma ocean [*Borg and Draper*, 2003]. But this Martian KREEP identified in meteorites does not reach the high K/Na observed among the Bradbury assemblage and is therefore not consistent with these rocks.

[60] Another possibility is that the K enrichment of the Bradbury rocks represents a mantle metasomatic event, involving solid-state modification of mantle peridotite by material transfer through a vapor or fluid (silicate liquid, water, Cl, CO_2, or carbonate [e.g., *Bailey*, 1982; *Pilet et al*., 2008; *McCubbin et al*., 2013]). Metasomatized mantle may contain hydrous K-bearing minerals like phlogopite and amphibole, which tend to melt first during partial melting to produce K-rich basaltic melts.

[61] Support for a metasomatized mantle origin for the Bradbury rocks comes from the modeled parent magmas of the nakhlite Martian meteorites that are also significantly enriched in K, with K_2O, Na_2O, and K/Na (Figure 6c [*Goodrich et al*., 2012, 2013]). In the nakhlites, the short-lived ^{146}Sm-^{142}Nd and long-lived ^{147}Sm-^{143}Nd radioisotope systems indicate that their mantle source region was enriched in light REEs (LREEs), which were themselves derived from long-term LREE-depleted source [*Borg et al*., 2003]. This constraint for the nakhlites is also not consistent with a KREEP component, which should not be depleted in LREE [e.g., *Warren and Wasson*, 1979], but is consistent with mantle metasomatism, whereby incompatible-element-enriched fluids or melts would have been derived from a depleted mantle source [*Borg et al*., 2003]. This process requires strong enrichment in incompatible elements in discrete domains, such as is seen in metasomatized terrestrial mantle and which has been ascribed to reactive transport [e.g., *Arai et al*., 1997; *Reiners*, 1998]. It seems reasonable that this inference may also apply to the Bradbury rocks, particularly given the limited alkaline compositions found so far on Mars. *McCubbin et al*. [2013] recently suggested that bulk compositions of the nakhlites (and particularly their apatites) imply late assimilation and degassing of a Cl-rich fluid. It would be difficult to recognize such a process in Bradbury rocks from their Cl contents alone given the wide distribution of Cl on the Martian surface.

[62] A heterogeneous distribution of K in the Martian interior has been previously suggested to explain the elevated K found in the Gusev basalts by the Spirit rover relative to the SNC meteorites by mantle processes [*Schmidt and McCoy*, 2010]. Also, the alkaline and evolved Jake_Matijevic rock is interpreted to have formed by low-degree partial melting of alkali-enriched mantle that was likely metasomatized by a K-rich fluid [*Stolper et al*., 2013]. Among the shergottitic meteorites and Gusev basalts, estimates for magmatic oxygen fugacity generally correlate with incompatible-element enrichment [e.g., *Herd et al*., 2002; *Schmidt et al*., 2013], which indicates multiple oxidation states in the Martian interior. We speculate that the enrichment in K of the Bradbury assemblage relative to other Martian rocks may point toward partial melting of an even more incompatible-element-rich, metasomatized, and possibly oxidized mantle source than is indicated by the Martian meteorites or by previous landed mission data sets.

6. Conclusions

[63] Although only early in the mission, it is already clear that the Curiosity rover landed in a lithologically diverse, K-rich region of Mars. The first four rocks examined by the APXS during the first 102 sols expand the range of Martian rock compositions to include high alkali and moderately volatile contents (up to 2.9 wt % K_2O and 1330 ppm Zn) with high Fe and Mn (up to 26.3 wt % FeO*). We interpret these rocks to be volcanic and/or relatively immature volcaniclastic sediments in origin. An apparent chemical mixing trend among three of the four rocks between Na + Al-rich and Fe + Zn-rich components is consistent with mechanical mixing by some type of sedimentary process.

[64] The unique chemistry of rocks at Gale crater relative to other sites of which we have knowledge on Mars suggests that we will need to refine models for volcanism and aqueous alteration. A lack of correlation between moderately volatile metals and Cl and S implies that models for oxidation and acidic alteration developed for the MER landing sites may not apply at Gale Crater for at least part of its geologic history. The high alkali signature of the Bradbury assemblage is likely derived from the rocks' source region, where the crust may have formed by low-degree partial melting of a metasomatized mantle. Very high iron in one of these rocks (Et_Then) may reflect the presence of iron-rich cements or

coatings that precipitated in the presence of an aqueous fluid. These findings bode well for the future richness of science discoveries as Curiosity continues its geologic traverse to Mt. Sharp.

[65] **Acknowledgments.** This work was funded by the Canadian Space Agency (CSA) support for the APXS instrument and Participating Scientist grant to Schmidt, and by the NASA MSL mission. Thoughtful reviews by Brian Balta, Cerena Goodrich, and Christian Schrader improved the manuscript. We sincerely thank the many engineers and scientists who have contributed to the great success of the MSL mission.

References

Agee, C. B., et al. (2013), Unique meteorite from early Amazonian Mars: Water-rich basaltic breccia Northwest Africa 7034, *Science*, *339*, 780–785.

Anderson, R. B., and J. F. Bell (2010), Geologic mapping and characterization of Gale Crater and implications for its potential as a Mars Science Laboratory landing site, *Mars*, *5*, 76–128, doi:10.1555/mars.2010.0004.

Arai, S., K. Matsukage, E. Isobe, and S. Ysotskiy (1997), Concentration of incompatible elements in oceanic mantle: Effect of melt/wall interaction in stagnant or failed melt conduits within peridotite, *Geochim. Cosmochim. Acta*, *61*, 671–675.

Bailey, D. K. (1982), Mantle metasomatism-continuing chemical change within the Earth, *Nature*, *296*, 525–530.

Beard, J. S., and G. E. Lofgren (1991), Dehydration melting and water-saturated melting of basaltic and andesitic greenstones and amphibolites at 1, 3, and 6.9 kbar, *J. Petrol.*, *32*, 365–401.

Berger, J. A., P. L. King, R. Gellert, J. L. Campbell, N. Boyd, I. Pradler, and G. M. Perrett, APXS and MSL Science Teams (2013), MSL titanium observation tray measurements with APXS Lunar and Planet. Sci. Con. 44, abs. 1321.

Blake, D. F., et al. (2013), Curiosity at Gale crater, Mars: Characterization and analysis of the Rocknest sand shadow, *Science*, *341*, doi:10.1126/science.1239505.

Blaney, D. L., et al. (2013), Assessment of potential rock coatings at Rocknest, Gale Crater with ChemCam, Lunar Planet. Sci. Con. 44, abs# 1568.

Borg, L. E., and D. S. Draper (2003), A petrogenetic model for the origin and compositional variation of the Martian basaltic meteorites, *Meteorit. Planet. Sci.*, *38*, 1713–1731.

Borg, L. E., L. E. Nyquist, H. Wiesmann, C.-Y. Shih, and Y. Reese (2003), The age of Dar al Gani 476 and the differentiation history of the Martian meteorites inferred from their radiogenic isotopic systematics, *Geochim. Cosmochim. Acta*, *67*, 3519–3536.

Brückner, J., G. Dreibus, R. Rieder, and H. Wänke (2003), Refined data of Alpha Proton X-ray Spectrometer analyses of soils and rocks at the Mars Pathfinder site: Implications for surface chemistry, *J. Geophys. Res.*, *108*(E12), 8094, doi:10.1029/2003JE002060.

Calef, F. J., III et al. (2013), Geologic mapping of the Mars Science Laboratory landing ellipse. Lunar Planetary Science Convention 44, abs. #2511.

Campbell, J. L. (2012), The instrumental blank of the Mars Science Laboratory alpha particle X-ray spectrometer, *Nucl. Instrum. Methods Phys. Res., Sect. B*, *288*, 102–110.

Campbell, J. L., G. M. Perrett, R. Gellert, S. M. Andrushenko, N. L. Boyd, J. A. Maxwell, P. L. King, and C. D. M. Schofield (2012), Calibration of the Mars Science Laboratory Alpha Particle X-ray Spectrometer, *Space Sci. Rev.*, *170*, 319–340.

Campbell, J. L., J. A. Berger, R. Gellert, P. L. King, G. M. Perret, N. I. Boyd, K. S. Edgett, R. A. Yingst, and MSL Science Team (2013), First measurements of the MSL APXS calibration target on Mars. Lunar Planet. Sci. Con. 44, abs. #1506.

Chan, M. A., W. T. Parry, and J. R. Bowman (2000), Diagenetic hematite and manganese oxides and fault-related fluid flow in Jurassic sandsones, southeastern Utah, *AAPG Bull.*, *84*, 1281–1310.

Clegg, S. M., E. Sklute, M. D. Dyar, J. E. Barefield, and R. C. Wiens (2009), Multivariate analysis of remote laser-induced breakdown spectroscopy spectra using partial least squares, principal component analysis, and related techniques, *Spectrochim. Acta Part B*, *64*, 79–88.

Debaille, V., Q.-Z. Yin, A. D. Brandon, and B. Jacobsen (2008), Martian mantle mineralogy investigated by the ^{176}Lu–^{176}Hf and ^{147}Sm–^{143}Nd systematics of shergottites, *Earth Planet. Sci. Lett.*, *269*, 186–199.

Debaille, V., A. D. Brandon, C. O'Neill, Q. Z. Yin, and B. Jacobsen (2009), Early Martian mantle overturn inferred from isotopic composition of nakhlite meteorites, *Nat. Geosci.*, *2*, 548–552.

Dixon, J. C., C. E. Thorn, R. G. Darmody, and S. W. Campbell (2002), Weathering rinds and rock coating from an arctic alpine environment, northern Scandinavia, *GSA Bull.*, *114*, 226–238.

Dreibus, G., and H. Wänke (1985), Mars, a volatile-rich planet, *Meteoritics*, *20*, 367–381.

Edgett, K. S., et al. (2012), Curiosity's Mars Hand Lens Imager (MAHLI) investigation, *Space Sci. Rev.*, *170*, 259–317.

Filiberto, J., and A. H. Treiman (2009), Martian magmas contained abundant chlorine, but little water, *Geology*, *37*, 1087–1090.

Forni, O., S. Maurice, O. Gasnault, R. C. Wiens, A. Cousin, S. M. Clegg, J.-B. Sirven, and J. Lasue (2013), Independent component analysis classification of laser induced breakdown spectroscopy spectra, *Spectrochim. Acta Part B*, doi:10.1016/j.sab.2013.05.003.

Frost, B. R., and C. D. Frost (2008), A geochemical classification for feldspathic igneous rocks, *J. Petrol.*, *49*, 1955–1969, doi:10.1093/petrology/egn054.

Gellert, R., et al. (2006), Alpha Particle X-ray Spectrometer (APXS): Results from Gusev crater and calibration report, *J. Geophys. Res.*, *111*, E02S05, doi:10.1029/2005JE002555.

Gellert, R., et al. (2013) Initial MSL APXS activities and observations at Gale Crater, Mars. Lunar Planet. Sci. Con. 44 Abs. #1432.

Goodrich, C. A., A. H. Treiman, J. Filiberto, J. Gross, and M. J. Jercinovic (2012), K-rich melt from the Martian mantle? Lunar and Planetary Science 43rd, Abs.# 1276.

Goodrich, C. A., A. H. Treiman, J. Filiberto, J. Gross, and M. Jercinovic (2013), K_2O-rich trapped melt in olivine in the Nakhla meteorite: Implications for the petrogenesis of nakhlites and differentiation of the Martian mantle, *Meteorit. Planet. Sci.*, *48*, 2371–2405.

Grotzinger, J. P., and R. E. Milliken (2012), The sedimentary rock record of Mars: Distribution, origins, and global stratigraphy, in *Sedimentary Geology of Mars*, edited by J. P. Grotzinger and R. E. Milliken, pp. 1–48, SEPM Special Paper, Tulsa, Okla.

Grotzinger, J. P., et al. (2012), Mars Science Laboratory mission and science investigation, *Space Sci. Rev.*, *170*, 5–56.

Grotzinger, J. P., et al. (2013), A habitable fluvio-lacustrine environment at Yellowknife Bay, Gale Crater, Mars, *Science*, doi:10.1126/science.1242777.

Halliday, A. N., H. Wänke, J.-L. Birck, and R. N. Clayton (2001), The accretion, composition and early differentiation of Mars, *Space Sci. Rev.*, *96*, 197–230.

Harri, A.-M., et al. (2013), Mars Science Laboratory (MSL)—First results of pressure and humidity observations. Lunar Planet. Sci. Con. 44, abs#1482.

Herd, C. D. K., L. E. Borg, J. H. Jones, and J. J. Papike (2002), Oxygen fugacity and geochemical variations in the Martian basalts: Implications for Martian basalt petrogenesis and the oxidation state of the upper mantle of Mars, *Geochim. Cosmochim. Acta*, *66*, 2025–2036.

Hurowitz, J. A., S. M. McLennan, N. J. Tosca, R. E. Arvidson, J. R. Michalski, D. W. Ming, C. Schröder, and S. W. Squyres (2006), In situ and experimental evidence for acidic weathering of rocks and soils on Mars, *J. Geophys. Res.*, *111*, E02S19, doi:10.1029/2005JE002515.

Jones, J. H. (2003), Constraints on the structure of the Martian interior determined from the chemical and isotopic systematics of SNC meteorites, *Meteorit. Planet. Sci.*, *38*, 1807–1814.

Kawabata, H., T. Hanyu, Q. Chang, J.-I. Kimura, R. L. Nichols, and Y. Tatsumi (2011), The petrology and geochemistry of St. Helena alkali basalts: Evaluation of the oceanic crust-recycling model for HIMU OIB, *J. Petrol.*, *52*, 791–838.

Kerber, L., J. W. Head, J.-B. Madeleine, F. Forget, and L. Wilson (2011), The dispersal of pyroclasts from Apollinaris Patera, Mars: Implications for the origin of the Medusae Fossae Formation, *Icarus*, *216*, 212–220.

Lanza, N. L., et al. (2013), Evidence for rock surface alteration with ChemCam from Curiosity's first 90 sols. Lunar Planet. Sci. Con. 44, abs. #1723.

Lasue, J., et al. (2013), Partial least squares sensitivity analysis and improvements for ChemCam LIBS data analysis on Mars. Lunar Planet. Sci. Con. 44, abs. #2230.

Le Bas, M. J., R. W. Le Maitre, A. Streckeisen, and B. Zanettin (1986), A chemical classification of volcanic rocks based on the total alkali-silica diagram, *J. Petrol.*, *27*, 745–750.

Leshin, L. A., et al. (2013), The first volatile, isotope, and organic analysis of solid samples with the Mars Curiosity Rover: Insights into Martian Fines, *Science*, *341*, doi:10.1126/science.1238937.

Lodders, K., and B. Fegley Jr. (1997), An oxygen isotope model for the composition of Mars, *Icarus*, *126*, 373–394.

Maurice, S., et al. (2012), The ChemCam instrument suite on the Mars Science Laboratory (MSL) Rover: Science objectives and mast unit description, *Space Sci. Rev.*, *170*, 95–166, doi:10.1007/s11214-012-9912-2.

McCubbin, F. M., S. M. Elardo, C. K. Shearer, A. Smirnov, E. H. Hauri, and D. S. Draper (2013), A petrogenetic model for the comagmatic origin of chassignites and nakhlites: Inferences from chlorine-rich minerals, petrology, and geochemistry, *Meteorit. Planet. Sci.*, *48*, 819–853.

McLennan, S. M., et al. (2013), Elemental geochemistry of sedimentary rocks at Yellowknife Bay, Gale Crater, Mars, *Science*, doi:10.1126/science.1244734.

McSween, H. Y., Jr., G. J. Taylor, and M. B. Wyatt (2009), Elemental composition of the Martian crust, *Science*, *324*, 736–739.
Meslin, P. Y., et al. (2013), Soil diversity and hydration as observed by ChemCam at Gale Crater, Mars, *Science*, *341*, doi:10.1126/science.1238670.
Meyer, C. (2013), The Martian Meteorite Compendium, http://curator.jsc.nasa.gov/antmet/mmc/index.cfm.
Mezger, K., V. Debaille, and T. Kleine (2013), Core and mantle differentiation on Mars, *Space Sci. Rev.*, *174*, 27–48.
Milliken, R. E., J. P. Grotzinger, and B. J. Thomson (2010), Paleoclimate of Mars as captured by the stratigraphic record in Gale Crater, *Geophys. Res. Lett.*, *37*, L04201, doi:10.1029/2009GL041870.
Ming, D. W., et al. (2008), Geochemical properties of rocks and soils in Gusev crater, Mars: Results of the Alpha Particle X-ray Spectrometer from Cumberland Ridge to Home Plate, *J. Geophys. Res.*, *113*, E12S39, doi:10.1029/2008JE003195.
Minitti, M. E., et al. (2013), Mars Hand Lens Imager (MAHLI) observations of rocks at Curiosity's field site, sols 0–100 Lunar Planet. Sci. Con. 44 Abs. #2186.
Morford, J. L., and S. Emerson (1999), The geochemistry of redox sensitive trace metals in sediments, *Geochim. Cosmochim. Acta*, *63*, 1735–1750.
Morris, R. V., et al. (2008), Iron mineralogy and aqueous alteration from Husband Hill through Home Plate at Gusev Crater, Mars: Results from the Mössbauer instrument on the Spirit Mars Exploration Rover, *J. Geophys. Res.*, *113*, E12S42, doi:10.1029/2008JE003201.
Nekvasil, H., A. Dondolini, J. Horn, J. Filiberto, H. Long, and D. H. Lindsley (2004), The origin and evolution of silica-saturated alkalic suites: An experimental study, *J. Petrol.*, *45*, 693–721.
Nesbitt, H. W., and R. E. Wilson (1992), Recent chemical weathering of basalts, *Am. J. Sci.*, *292*, 740–777.
Ollila, A. M., et al. (2013a), Early results from Gale Crater on ChemCam detections of carbon, lithium, and rubidium Lunar Planet. Sci. Con. 44, Abs. #2188.
Ollila, A., et al. (2013b), Modeling of minor and trace elements (Li, Ba, Sr, Rb, Mn, and C) using Curiosity's ChemCam and early results for Gale Crater from Bradbury Landing to Rocknest, *J. Geophys. Res. Planets*, *119*, 255–285, doi:10.1002/2013JE004517.
Palucis, M. C., W. E. Dietrich, A. Hayes, R. M. E. Williams, F. Calef, D. Y. Sumner, S. Gupta, C. Hardgrove, and MSL Science Team (2013), Origin and evolution of the Peace Vallis Fan system that drains the Curiosity landing area, Gale Crater Lunar Planet. Sci. Con. 44 Abs. #1607.
Pilet, S., M. B. Baker, and E. S. Stolper (2008), Metasomatized lithosphere and the origin of alkaline lavas, *Science*, *320*, 916–919.
Reiners, P. W. (1998), Reactive melt transport in the mantle and geochemical signatures of mantle-derived magmas, *J. Petrol.*, *39*, 1039–1061.
Rice, M. S., J. M. Williams, F. Calef, R. B. Anderson, L. Edgar, K. Stack, D. Y. Sumner, H. E. Newsom, J. P. Grotzinger, and P. King (2013), Detailed geologic mapping along the Mars Science Laboratory (MSL) Curiosity traverse path from Glenelg to Mount Sharp. Lunar Planetary Science Conference 44, abs. #2892.
Rieder, R., et al. (2004), Chemistry of rocks and soils at Meridiani Planum from the Alpha Particle X-ray Spectrometer, *Science*, *306*, 1746–1749.
Righter, K., K. Pando, and L. R. Danielson (2009), Experimental evidence for sulfur-rich Martian magmas: Implications for volcanism and surficial sulfur sources, *Earth Planet. Sci. Lett.*, *288*, 235–243.
Sautter, V. et al. (2014), Igneous mineralogy at Bradbury rise: The first ChemCam campaign, *J. Geophys. Res. Planets*, *119*, 30–46, doi:10.1002/2013JE004472.
Schmeling, H. (2000), Partial melting and melt segregation in a convecting mantle *in* Bagdassrov, N.S., Laporte, D., Thompson, A.B., eds. Physics and Chemistry of Partially Molten Rocks, *Petrol. Struct. Geol.*, *111*, 141–178.
Schmidt, M. E., and T. J. McCoy (2010), The evolution of a heterogeneous Martian mantle: Clues from K, P, Ti, Cr, and Ni variations in Gusev basalts and shergottite meteorites, *Earth Planet. Sci. Lett.*, *296*, 67–77, doi:10.1016/j.epsl.2010.04.046.
Schmidt, M. E., et al. (2009), Spectral, mineralogical, and geochemical variations across Home Plate, Gusev Crater, Mars indicate high and low temperature alteration, *Earth Planet. Sci. Lett.*, *281*, 258–266.
Schmidt, M. E., C. M. Schrader, and T. J. McCoy (2013), The primary fO_2 of basalts examined by the Spirit Rover in Gusev Crater, Mars: Evidence for multiple redox states in the Martian interior, *Earth Planet. Sci. Lett.*, *384*, 198–208.
Scott, D. H., and M. G. Chapman (1995), Geologic and topographic maps of the Elysium Paleolake Basin, Mars. USGS Misc. Map, I-2397, scale 1:5,000,000.
Smith, P. H., et al. (2009), H_2O at Phoenix landing site, *Science*, *325*, 58–61.
Squyres, S. W., et al. (2004a), The Spirit Rover's Athena science investigation at Gusev Crater, Mars, *Science*, *305*, 794–799.
Squyres, S. W., et al. (2004b), In situ evidence for an ancient aqueous environment at Meridiani Planum, Mars, *Science*, *306*, 1709–1714.
Squyres, S. W., et al. (2006), Rocks of the Columbia Hills, *J. Geophys. Res.*, *111*, E02S11, doi:10.1029/2005JE002562.
Squyres, S. W., et al. (2012), Ancient impact and aqueous processes at Endeavour Crater, Mars, *Science*, *336*, 570–576.
Stolper, E. M., et al. (2013), The petrochemistry of Jake_M: A Martian mugearite, *Science*, *341*, doi:10.1126/science.1239463.
Sumner, D. Y., et al. (2013), Preliminary geological map of the Peace Vallis Fan integrated with in situ mosaics from the Curiosity Rover, Gale Crater, Mars. Lunar Planetary Science Conference abs. #1699.
Sun, S. S., and W. McDonough (1989), Chemical and isotopic systematics of oceanic basalts: Implications for mantle composition and processes, *Geol. Soc. London Spec. Publ.*, *42*, 313–345.
Taylor, S. R., and S. M. McLennan (2009), *Planetary Crusts: Their Composition, Origin and Evolution*, pp. 378, Cambridge Univ. Press, Cambridge.
Thompson, L. M., et al. (2013), BT-2 calibration target for the Mars Science Laboratory Alpha Particle X-ray Spectrometer: Characterization and alkali basalt Martian analogue. Lunar Planet. Sci. Con. 44 Abs. #2190.
Thomson, B. J., N. T. Bridges, R. Milliken, A. Baldridge, S. J. Hook, J. K. Crowley, G. M. Marion, C. R. de Souza Filho, A. J. Brown, and C. M. Weitz (2011), Constraints on the origin and evolution of the layered mound in Gale Crater, Mars using Mars Reconnaissance Orbiter data, *Icarus*, *214*, 413–432.
Tokar, R. L., et al. (2013), Searching for chemical variation across the surface of "Rocknest_3" using MSL ChemCam spectra. Lunar Planet. Sci. Con. 44 Abs#1283.
Treiman, A. H. (2003), Chemical compositions of Martian basalts (shergottites): Some inferences on basalt formation, mantle metasomatism, and differentiation in Mars, *Meteorit. Planet. Sci.*, *38*, 1849–1864.
Usui, T., H. Y. McSween Jr., and B. C. Clark III (2008), Petrogenesis of high-phosphorous Wishstone-class rocks in Gusev crater, Mars, *J. Geophys. Res.*, *113*, E12S44, doi:10.1029/2008JE003225.
Walker, T. R., E. E. Larson, and R. P. Hoblitt (1981), Nature and origin of hematite in the Moenkopi formation (Triassic) Colorado Plateau: A contribution to origin of magnetism in red beds, *J. Geophys. Res.*, *86*, 317–333.
Wänke, H., and G. Dreibus (1988), Chemical composition and accretion history of terrestrial planets, *Philos. Trans. R. Soc. London*, *A325*, 545–557.
Warren, P. H., and J. T. Wasson (1979), The origin of KREEP, *Rev. Geophys. Space Phys.*, *17*, 73–88.
Whitaker, M. L., H. Nekvasi, D. H. Lindsley, and N. J. Difrancesco (2007), The role of pressure in producing compositional diversity in intraplate basaltic magmas, *J. Petrol.*, *48*, 365–393.
Wiens, R. C., et al. (2012), The ChemCam instrument suite on the Mars Science Laboratory (MSL) Rover: Body unit and combined system tests, *Space Sci. Rev.*, *170*, 167–227.
Wiens, R. C., et al. (2013), Pre-flight calibration and initial data processing for the ChemCam laser-induced breakdown spectroscopy instrument on the Mars Science Laboratory Rover, *Spectrochim. Acta Part B*, *82*, 1–27.
Williams, R. M. E., et al. (2013), Martian fluvial conglomerates at Gale Grater, *Science*, *340*, 1068–1072.
Yen, A. S., et al. (2005), An integrated view of the chemistry and mineralogy of Martian soils, *Nature*, *436*, 49–54.
Yen, A. S., et al. (2013), Evidence for a global Martian soil composition extends to Gale Crater. Lunar Planet. Sci. Con. 44 Abs. #2495.
Zimbelman, J. R., and S. P. Scheidt (2012), Hesperian Age for Western Medusae Fossae Formation, Mars, *Science*, *336*, 1683–1683.
Zipfel, J., et al. (2011), Bounce Rock—A shergottite-like basalt encountered in Meridiani Planum, Mars, *Meteorit. Planet. Sci.*, *46*, 1–20.